IEEE TRANSACTIONS ON

AEROSPACE AND ELECTRONIC SYSTEMS

APRIL 2015 VOLUME 51 NUMBER 2 ISSN 0018-9251

A QUARTERLY PUBLICATION OF THE IEEE AEROSPACE AND ELECTRONIC SYSTEMS SOCIETY

Contents continued on back cover

IEEE TRANSACTIONS ON AEROSPACE AND ELECTRONIC SYSTEMS Volume 51, No. 2 April 2015

Contents continued from cover 1

CORRESPONDENCE

Subspace-Based Two-Dimensional Direction Estimation and Tracking of Multiple Targets

GUANGMIN WANG, Student Member, IEEE
JINGMIN XIN, Senior Member, IEEE
Xi'an Jiaotong University
Xi'an, China

JIASONG WANG
State Key Laboratory of Astronautic Dynamics
Xi'an, China

NANNING ZHENG, Fellow, IEEE
Xi'an Jiaotong University
Xi'an, China

AKIRA SANO, Member, IEEE
Keio University
Yokohama, Japan

This paper deals with the problem of tracking the two-dimensional (2-D) direction-of-arrivals (DOAs) of multiple moving targets with crossover points on their trajectories, and we propose a new computationally efficient cross-correlation based 2-D DOA estimation with automatic pair-matching (CODEC) method for noncoherent narrowband signals impinging on the L-shaped sensor array structured by two uniform linear arrays (ULAs) with omnidirectional sensors. The effectiveness of the proposed method and the theoretical analysis are substantiated through numerical examples.

Manuscript received January 10, 2013; revised May 12, 2014; released for publication August 17, 2014.

DOI. No. 10.1109/TAES.2014.130018.

Refereeing of this contribution was handled by T. Luginbuhl.

This work was supported in part by the National Natural Science Foundation of China under Grants 61172162 and 61231018, the Programme of Introducing Talents of Discipline to Universities under Grant B13043, and the Specialized Research Fund for the Doctoral Program of Higher Education of China under Grant 20130201110016.

Authors' addresses: G. Wang, J. Xin, N. Zheng, the National Engineering Laboratory of Visual Information Processing and Applications and the Institute of Artificial Intelligence and Robotics, Xi'an Jiaotong University, Xi'an 710049, China. E-mail: (jxin@mail.xjtu.edu.cn; nnzheng@mail.xjtu.edu.cn). J. Xin, Xi'an Jiaotong University Suzhou Academy, Suzhou 215123, China; J. Wang, the State Key Laboratory of Astronautic Dynamics, Xi'an 710043, China; A. Sano, the Department of System Design Engineering, Keio University, Yokohama 223-8522, Japan. E-mail: (sano@sd.keio.ac.jp).

I. INTRODUCTION

The problem of tracking the two-dimensional (2-D) direction-of-arrivals (DOAs) (i.e., azimuth and elevation angles) of multiple moving targets is important in many practical applications of sensor array processing involved in radar, sonar, communications, and so on (cf. [1]). Because of the increase in the dimensionality, the 2-D DOA estimation and tracking are considerably more difficult than the 1-D problems [2], where the estimated azimuth angles should be associated with the corresponding elevation angles of the same incident signals. Compared with the optimal but computationally complicated maximum likelihood (ML) method (e.g., [3, 4]), various subspace-based suboptimal methods have been developed to solve such 2-D DOA estimation problems from their 1-D versions by using planar arrays such as the uniform circular or rectangular arrays (e.g., [5–15]). Although numerous algorithms for the 1-D DOA (i.e., azimuth angle) tracking have been devised in the literature (e.g., [16–19] and references therein), the problem of 2-D DOA tracking of multiple moving signals has not been extensively studied except for [20–22], where the difficulties are the pair-matching of the estimated azimuth and elevation angles and the association of these estimates at two successive time instants. By extending the 1-D recursive algorithm [23] or the gradient-based iterative searching algorithm [24] to 2-D scenarios, two different 2-D DOA tracking algorithms were proposed by using rectangular planar array [20, 21]. Even though the association of azimuth and elevation estimates is embedded in the estimation itself, these algorithms [21] require the multiple signal classification (MUSIC) method [26] with eigendecomposition to determine the noise variance, the signal covariance matrix, and the initial estimates of azimuth and elevation angles. Thus their tracking performances are affected by the accuracy of these parameters [23, 24], and they become poor at low signal-to-noise ratio (SNR). Additionally the joint 2-D DOA tracking algorithm [22, 25] still invokes the computationally expensive eigendecomposition procedure in DOA estimation and the minimization of a function for associating the azimuth/elevation estimates at each time instant, though the subspace updating is accomplished by employing the low-rank adaptive filters [27].

On the other hand, the computational complexity of 2-D DOA estimation and tracking is usually affected by the array geometric configurations, and these special configurations can be exploited to develop computationally efficient DOA estimation methods [28]. Especially an L-shaped array composed of two uniform linear arrays (ULAs) connected orthogonally at one end of each ULA (i.e., shifted cross array) has attained considerable attention, because it has some advantages in geometric configuration and implementation compared with the conventional planar array and higher estimation accuracy than other simple structured planar arrays consisting of two or more ULAs [29]. Many 2-D DOA

estimation methods with eigendecomposition were proposed for the L-shaped array placed in the x–y or x–z plane by exploiting the array configuration to decouple the conventional 2-D estimation problem into two independent 1-D estimation problems (e.g., [29–37]). Unfortunately, the existing pair-matching techniques are a computationally costly operation [5, 6, 10, 29, 36, 37], and they do not always provide the correct pairing results. Consequently, without considering the permissible region of the parameters in the estimation process, the pairing failure and erroneous estimate can cause the estimation failure (cf. [10] for details), where the estimated azimuth/elevation angle pair does not exist in the real world, or the angles cannot be calculated from the estimated auxiliary variables, which do not lie in their permissible region. Nevertheless the measure to combat the estimation failure described above has not been well studied in the existing 2-D DOA estimation methods for the L-shaped array (e.g., [29–35, 37]), while these methods involve the computationally intensive and time-consuming eigendecomposition process (cf. [38, 39]), and hence they may still be unapplicable for real-time implementation. In addition, we proposed a computationally efficient cross-correlation based 2-D DOA estimation (CODE) method without eigendecomposition for 2-D DOA estimation of noncoherent narrowband signals impinging on the L-shaped sensor array structured by two ULAs [40]. Although the effect of additive noises is mitigated, this batch CODE method needs a pair-matching procedure, which requires a tremendous computational burden when the number of incident signals is large. As a result, the CODE is still inapplicable for tracking the 2-D time-varying DOAs in real-time.

Therefore in this paper, we investigate the problem of tracking the 2-D DOAs of multiple moving targets with crossover points on their trajectories and propose a new computationally efficient subspace-based 2-D DOA tracking algorithm with the L-shaped sensor array, where the crux is to associate the estimated azimuth and elevation angles of different targets at two successive time instants (i.e., the so-called "data association" [1]). Based on the previous works [19] and [40], first a new computationally efficient cross-correlation based 2-D DOA estimation with automatic pair-matching (CODEC) batch method is developed for noncoherent narrowband signals, where the computationally expensive procedures of eigendecomposition in subspace estimation and pair-matching of the estimated azimuth and elevation angles are avoided. Another notable difference between the CODE and CODEC methods is that the azimuth angles are estimated with different cross-correlations and working array aperture. Then the on-line implementation of the proposed CODEC method is presented for tracking the 2-D DOAs of multiple moving targets with crossover points on their trajectories, where the association of the estimated azimuth and elevation angles at two successive time instants is accomplished by employing a dynamic model and the Luenberger state observer [41]. As a result,

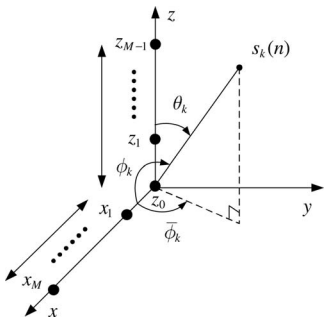

Fig. 1. Geometrical configuration of L-shaped array for 2-D direction estimation [37].

the CODEC method has two notable advantages over the previously proposed CODE method [40]: an automatic pairing procedure is introduced to reduce the overall computational complexity of the estimation and a 1-D tracking algorithm is extended to the 2-D tracking of multiple targets with crossover points on their trajectories. Moreover, the asymptotic mean-square-error (MSE) expressions of the azimuth and elevation estimates are derived explicitly. The effectiveness of the batch CODEC method and its theoretical analysis are verified through numerical examples, and the simulation results also show that the proposed tracking algorithm has good adaptability and tracking capability.

II. PROBLEM FORMULATION

A. Basic Notation

The following notational conventions are used throughout this paper: the italic letters, lower-case boldface letters, and capital boldface letters indicate the scalars, column vectors, and matrices, and $\boldsymbol{O}_{m\times n}$, $\boldsymbol{I}_m$, $\boldsymbol{J}_m$, $\boldsymbol{0}_{m\times 1}$, and $\delta_{n,t}$ denote the $m \times n$ null matrix, $m \times m$ identity matrix, $m \times m$ counter-identity matrix, $m \times 1$ null vector, and Kronecker delta, while $E\{\cdot\}$, $(\cdot)^*$, $(\cdot)^T$, and $(\cdot)^H$ represent the statistical expectation, complex conjugation, transposition, and Hermitian transposition, respectively. Additionally $\hat{x}$ means the estimate of the variable x, while $\mathrm{diag}\{\cdot\}$, $\det\{\cdot\}$, and $\mathrm{Re}\{\cdot\}$ denotes the diagonal operation, determinant of a matrix, and real part of the quantity.

B. Data Model

The L-shaped sensor array is placed in the x–z plane and consists of two ULAs as depicted in Fig. 1, where each ULA has M omnidirectional sensors with spacing d, the sensor at the origin of coordinates z_0 is the reference one for each ULA, and the interelement spacing between the sensors z_0 and x_1 of these ULAs is also d. Here we suppose that p noncoherent narrowband signals $\{s_k(n)\}$ from multiple targets with the wavelength λ are in the far-field and impinge on the array from distinct directions with the elevation and azimuth angles $(\theta_k(n), \phi_k(n))$ [29, 37], where $\theta_k(n) \neq \theta_i(n)$ and $\phi_k(n) \neq \phi_i(n)$ for $k \neq i$. As illustrated in Fig. 1, the elevation angle $\theta_k(n)$ and the azimuth angle $\phi_k(n)$ are measured clockwise relative to the

z or x axis, while the projected azimuth angle $\bar{\phi}_k(n)$ is measured counterclockwise relative to the x axis in the x–y plane, where $0^\circ \le \theta_k(n) \le 180^\circ$, $0^\circ \le \phi_k(n) \le 180^\circ$, and $0^\circ \le \bar{\phi}_k(n) \le 180^\circ$. Then the received signals at two ULAs are given by

$$\boldsymbol{z}(n) = \boldsymbol{A}(\theta)\boldsymbol{s}(n) + \boldsymbol{w}_z(n) \tag{1}$$

$$\boldsymbol{x}(n) = \boldsymbol{A}(\phi)\boldsymbol{s}(n) + \boldsymbol{w}_x(n) \tag{2}$$

where $\boldsymbol{z}(n) \triangleq [z_0(n), z_1(n), \cdots, z_{M-1}(n)]^T$, $\boldsymbol{x}(n) \triangleq [x_1(n), x_2(n), \cdots, x_M(n)]^T$, $\boldsymbol{w}_z(n) \triangleq [w_{z_0}(n), w_{z_1}(n), \cdots, w_{z_{M-1}}(n)]^T$, $\boldsymbol{w}_x(n) \triangleq [w_{x_1}(n), w_{x_2}(n), \cdots, w_{x_M}(n)]^T$, $\boldsymbol{s}(n) \triangleq [s_1(n), s_2(n), \cdots, s_p(n)]^T$, $\boldsymbol{A}(\theta) \triangleq [\boldsymbol{a}(\theta_1(n)), \boldsymbol{a}(\theta_2(n)), \cdots, \boldsymbol{a}(\theta_p(n))]$, $\boldsymbol{a}(\theta_k(n)) \triangleq [1, e^{j\alpha_k(n)}, \cdots, e^{j(M-1)\alpha_k(n)}]^T$, $\boldsymbol{A}(\phi) \triangleq [\boldsymbol{a}(\phi_1(n)), \boldsymbol{a}(\phi_2(n)), \cdots, \boldsymbol{a}(\phi_p(n))]$, $\boldsymbol{a}(\phi_k(n)) \triangleq [e^{j\beta_k(n)}, e^{j2\beta_k(n)}, \cdots, e^{jM\beta_k(n)}]^T$, $\alpha_k(n) \triangleq 2\pi d \cos(\theta_k(n))/\lambda$, and $\beta_k(n) \triangleq 2\pi d \cos(\phi_k(n))/\lambda$.

In this paper, the following basic assumptions are made on the data model.

A1) The mathematical model of array response matrices (i.e., $\boldsymbol{A}(\theta)$ and $\boldsymbol{A}(\phi)$) is known, and the sensor spacing d satisfies $0 < d \le \lambda/2$ to avoid angle ambiguity.

A2) For facilitating the theoretical performance analysis, the incident signals $\{s_k(n)\}$ are temporally complex white Gaussian random processes with zero-mean and the variance are given by $E\{s_k(n)s_k^*(t)\} = r_{s_k}\delta_{n,t}$ and $E\{s_k(n)s_k(t)\} = 0 \forall n, t$ for $1 \le k \le p$.

A3) The additive noises $\{w_{z_i}(n)\}$ and $\{w_{x_i}(n)\}$ are temporally and spatially complex white Gaussian random processes with zero-mean and the covariance matrices are given by $E\{\boldsymbol{w}_z(n)\boldsymbol{w}_z^H(t)\} = E\{\boldsymbol{w}_x(n)\boldsymbol{w}_x^H(t)\} = \sigma^2\boldsymbol{I}_M\delta_{n,t}$, and $E\{\boldsymbol{w}_z(n)\boldsymbol{w}_z^T(t)\} = E\{\boldsymbol{w}_x(n)\boldsymbol{w}_x^T(t)\} = \boldsymbol{O}_{M\times M}\forall n, t$, and they are statistically independent with each other, i.e., $E\{\boldsymbol{w}_z(n)\boldsymbol{w}_x^H(t)\} = \boldsymbol{O}_{M\times M}$.

A4) The additive noises $\{w_{z_i}(n)\}$ and $\{w_{x_i}(n)\}$ at two ULAs are statistically independent with the incident signals $\{s_k(n)\}$.

A5) The number of incident signals p is known or estimated by number detection techniques in advance (cf. [42, 43], and it satisfies the inequality that $p < M$.

From the relationship $\cos(\phi_k(n)) = \cos(\bar{\phi}_k(n)) \times \sin(\theta_k(n))$ [10, 37], we easily find the permissible region for $\theta_k(n)$ and $\phi_k(n)$ and for $\theta_k(n)$ and $\bar{\phi}_k(n)$ as shown in Figs. 2(a) and 2(b), respectively, while the geometry restrictions require that the parameters $\theta_k(n)$ and $\phi_k(n)$ lie in the square region defined by

$$\begin{aligned} -\theta_k(n) + 90^\circ \le \phi_k(n) &\le \theta_k(n) + 90^\circ, \\ &\text{for } 0^\circ \le \theta_k(n) \le 90^\circ \\ \theta_k(n) - 90^\circ \le \phi_k(n) &\le -\theta_k(n) + 270^\circ, \\ &\text{for } 90^\circ \le \theta_k(n) \le 180^\circ. \end{aligned} \tag{3}$$

The classical 1-D subspace-based direction estimation methods with eigendecomposition (e.g., MUSIC [26],

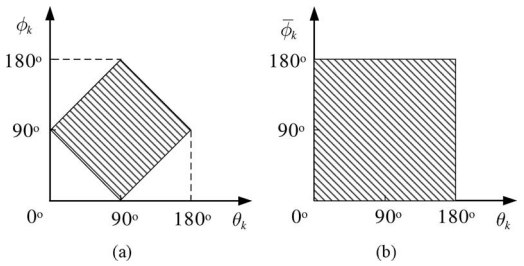

Fig. 2. Permissible regions for (a) elevation angle $\theta_k(n)$ and azimuth angle $\phi_k(n)$ and (b) elevation angle $\theta_k(n)$ and projected azimuth angle $\bar{\phi}_k$.

estimation of signal parameters via rational invariance techniques (ESPRIT) [44]) and the computationally simple 1-D subspace-based direction estimators without eigendecomposition (e.g., propagator method (PM) [45], subspace-based method without eigendecomposition (SUMWE) [39]) can be applied to each ULA to obtain the reliable estimates of azimuth and elevation angles separately. However, in general, there are $p!$ possible combinations between the estimates $\{\hat{\phi}_k(n)\}$ and $\{\hat{\theta}_i(n)\}$. Consequently the crux of 2-D direction estimation is the pair-matching of the azimuth and elevation angles estimated independently, which can require a tremendous computational burden when the number of incident signals is large. Except for the CODE [40], most of the existing techniques for pair-matching or automatic pairing involve the computationally extensive eigendecomposition process [5–8, 10, 29, 30, 32–34, 36, 37]. Even though the pair-matching is accomplished correctly, the separate estimation of the azimuth and elevation angles may cause the estimated angles $\hat{\theta}_k(n)$ and $\hat{\phi}_k(n)$ to lie outside the permissible region shown in Fig. 2(a), or equivalently we may have $|\cos(\hat{\phi}_k(n))/\sin(\hat{\theta}_k(n))| > 1$ for $\sin\hat{\theta}_k \ne 0$, and obviously the estimate of the conventional azimuth angle $\bar{\phi}_k(n)$ is unavailable with the relation $\bar{\phi}_k(n) = \arccos(\cos(\phi_k(n))/\sin(\theta_k(n)))$. Thus the estimation failure occurs in this situation [10]. Unfortunately, the estimation failure has not been resolved yet for the L-shaped array. Therefore in order to overcome the aforementioned pairing and estimation failures, we focus our attention on the joint azimuth-elevation DOA estimation without eigendecomposition process and pair-matching procedure.

REMARK 1 For decoupling the 2-D DOA estimation problem into 1-D estimation problems and fully exploiting the well-known property of the ULA in a more straightforward way, we parameterize the 2-D direction of the incident signals by $(\theta_k(n),\phi_k(n))$ instead of $(\theta_k(n), \bar{\phi}_k(n))$. In fact, by redefining the parameter $\theta_k(n)$ as the angle of the signal $s_k(n)$ with respect to the y axis, the proposed CODEC method is also applicable to the L-shaped array placed in the x–y plane. However in order to compare the performance of the CODEC method with the existing methods, we still concentrate on the problem of 2-D DOA estimation with L-shaped array placed in the x–z plane in this paper.

III. BATCH METHOD FOR 2-D DOA ESTIMATION

A. Estimation of Elevation Angles

Firstly by assuming the elevation and azimuth angles to be time invariant, i.e., $\theta_k(n) = \theta_k$ and $\phi_k(n) = \phi_k$, we can propose a new computationally efficient batch 2-D DOA estimation method without eigendecomposition and pair-matching, which is suitable for DOA tracking. Under assumption A5, we can divide the ULA along the z axis into two nonoverlapping forward subarrays with p or $M-p$ sensors, and the received signal vector $\boldsymbol{z}(n)$ in (1) can be rewritten as

$$\begin{aligned}\boldsymbol{z}(n) &= [\bar{\boldsymbol{z}}_1^T(n), \bar{\boldsymbol{z}}_2^T(n)]^T \\ &= [\boldsymbol{A}_1^T(\theta), \boldsymbol{A}_2^T(\theta)]^T \boldsymbol{s}(n) + [\boldsymbol{w}_{\bar{z}_1}^T(n), \boldsymbol{w}_{\bar{z}_2}^T(n)]^T \quad (4)\end{aligned}$$

where $\bar{\boldsymbol{z}}_1(n) \triangleq [z_0(n), z_1(n), \cdots, z_{p-1}(n)]^T$, $\bar{\boldsymbol{z}}_2(n) \triangleq [z_p(n), z_{p+1}(n), \cdots, z_{M-1}(n)]$, $\boldsymbol{w}_{\bar{z}_1}(n) \triangleq [w_{z_0}(n), w_{z_1}(n), \cdots, w_{z_{p-1}}(n)]^T$, and $\boldsymbol{w}_{\bar{z}_2}(n) \triangleq [w_{z_p}(n), w_{z_{p+1}}(n), \cdots, w_{z_{M-1}}(n)]^T$, while $\boldsymbol{A}(\theta)$ in (1) is divided into two submatrices $\boldsymbol{A}_1(\theta)$ and $\boldsymbol{A}_2(\theta)$ with the columns given by $\boldsymbol{a}_1(\theta_k) \triangleq [1, e^{j\alpha_k}, \cdots, e^{j(p-1)\alpha_k}]^T$ and $\boldsymbol{a}_2(\theta_k) \triangleq [e^{jp\alpha_k}, e^{j(p+1)\alpha_k}, \cdots, e^{j(M-1)\alpha_k}]^T$. Then under the assumptions of data model, from (1), (2), and (4), we easily obtain the cross-correlation matrix $\boldsymbol{R}_{zx}$ between the received signals of two ULAs along the $\boldsymbol{x}$ and $\boldsymbol{z}$ axes as

$$\begin{aligned}\boldsymbol{R}_{zx} &\triangleq E\{\boldsymbol{z}(n)\boldsymbol{x}^H(n)\} = [\boldsymbol{R}_{\bar{z}_1 x}^T, \boldsymbol{R}_{\bar{z}_2 x}^T]^T \\ &= \boldsymbol{A}(\theta) E\{\boldsymbol{s}(n)\boldsymbol{s}^H(n)\}\boldsymbol{A}^T(\phi) + E\{\boldsymbol{w}_z(n)\boldsymbol{w}_x^H(n)\} \\ &= \boldsymbol{A}(\theta)\boldsymbol{R}_s\boldsymbol{A}^H(\phi) \quad (5)\end{aligned}$$

where $\boldsymbol{R}_s$ is the source signal covariance matrix defined by $\boldsymbol{R}_s \triangleq E\{\boldsymbol{s}(n)\boldsymbol{s}^H(n)\}$, $\boldsymbol{R}_{\bar{z}_1 x} \triangleq E\{\bar{\boldsymbol{z}}_1(n)\boldsymbol{x}^H(n)\} = \boldsymbol{A}_1(\theta)\boldsymbol{R}_s\boldsymbol{A}^H(\phi)$, and $R_{\bar{z}_2 x} \triangleq E\{\bar{\boldsymbol{z}}_2(n)\boldsymbol{x}^H(n)\} = \boldsymbol{A}_2(\theta)\boldsymbol{R}_s\boldsymbol{A}^H(\phi)$. Similarly by partitioning the same ULA into two nonoverlapping backward subarrays composed of p and $M-p$ sensors, we can express the conjugate noisy signal vector $\tilde{\boldsymbol{z}}(n)$ of this ULA as

$$\begin{aligned}\bar{\boldsymbol{z}}(n) &\triangleq [\tilde{\boldsymbol{z}}_1^T(n), \tilde{\boldsymbol{z}}_2^T(n)]^T = \boldsymbol{J}_M \boldsymbol{z}^*(n) \\ &= \boldsymbol{A}(\theta)\boldsymbol{D}^{-(M-1)}(\theta)\boldsymbol{s}^*(n) + \tilde{\boldsymbol{w}}_z(n) \quad (6)\end{aligned}$$

where $\tilde{\boldsymbol{z}}_1(n) \triangleq [z_{M-1}(n), z_{M-2}, \cdots, z_{M-p}(n)]^H$, $\tilde{\boldsymbol{z}}_2(n) \triangleq [z_{M-p-1}(n), \cdots, z_1(n), z_0(n)]^H$, $\tilde{\boldsymbol{w}}_z(n) \triangleq [w_{z_{M-1}}(n), \cdots, w_{z_1}(n), w_{z_0}(n)]^H$, and $\boldsymbol{D}(\theta) \triangleq \mathrm{diag}(e^{j\alpha_1}, e^{j\alpha_2}, \cdots, e^{j\alpha_p})$. Then from (6) and (2), we can obtain another cross-correlation matrix $\tilde{\boldsymbol{R}}_{zx}$ as

$$\begin{aligned}\tilde{\boldsymbol{R}}_{zx} &\triangleq E\{\tilde{\boldsymbol{z}}(n)\boldsymbol{x}^T(n)\} = [\tilde{\boldsymbol{R}}_{\bar{z}_1 x}^T, \tilde{\boldsymbol{R}}_{\bar{z}_2 x}^T]^T \\ &= \boldsymbol{J}_M(E\{\boldsymbol{z}(n)\boldsymbol{x}^H(n)\})^* = \boldsymbol{J}_M\boldsymbol{R}_{zx}^* \\ &= \boldsymbol{A}(\theta)\boldsymbol{D}^{-(M-1)}(\theta)(E\{\boldsymbol{s}(n)\boldsymbol{s}^H(n)\})^*\boldsymbol{A}^T(\phi) \\ &\quad + E\{\tilde{\boldsymbol{w}}_z(n)\boldsymbol{w}_x^T(n)\} \\ &= \boldsymbol{A}(\theta)\boldsymbol{D}^{-(M-1)}(\theta)\boldsymbol{R}_s^*\boldsymbol{A}^T(\phi) \quad (7)\end{aligned}$$

where $\tilde{\boldsymbol{R}}_{\tilde{z}_1 x} \triangleq E\{\tilde{\boldsymbol{z}}_1(n)\boldsymbol{x}^T(n)\} = \boldsymbol{A}_1(\theta)\boldsymbol{D}^{-(M-1)}(\theta)\boldsymbol{R}_s^*\boldsymbol{A}^T(\phi)$, $\tilde{\boldsymbol{R}}_{\tilde{z}_2 x} \triangleq E\{\tilde{\boldsymbol{z}}_2(n)\boldsymbol{x}^T(n)\} = \boldsymbol{A}_2(\theta)\boldsymbol{D}^{-(M-1)}(\theta)\boldsymbol{R}_s^*\boldsymbol{A}^T(\phi)$. Obviously these matrices $\boldsymbol{R}_{zx}$ and $\tilde{\boldsymbol{R}}_{zx}$ are not affected by the additive noises at two ULAs.

From (4), (5), and (7), we can form an $M \times 2M$ extended cross-correlation matrix $\boldsymbol{R}_z$ as

$$\begin{aligned}\boldsymbol{R}_z &\triangleq [\boldsymbol{R}_{zx}, \tilde{\boldsymbol{R}}_{zx}] = [\boldsymbol{R}_{zx}, \boldsymbol{J}_M\boldsymbol{R}_{zx}^*] \\ &= [\boldsymbol{A}_1^T(\theta), \boldsymbol{A}_2^T(\theta)]^T[\boldsymbol{R}_s\boldsymbol{A}^H(\phi), \boldsymbol{D}^{-(M-1)}(\theta)\boldsymbol{R}_s^*\boldsymbol{A}^T(\phi)] \\ &\triangleq [\boldsymbol{R}_{z1}^T, \boldsymbol{R}_{z2}^T]^T \quad (8)\end{aligned}$$

where $\boldsymbol{R}_{z1}$ and $\boldsymbol{R}_{z2}$ are the submatrices consisting of the first p and the last $M-p$ rows of $\boldsymbol{R}_z$. Because the incident signals $\{s_k(n)\}$ come from distinct directions with the elevation and azimuth angles (θ_k, ϕ_k), by considering assumptions A1 and A5, we can obtain that the $M \times p$ array response matrix $\boldsymbol{A}(\theta)$ in (1) and its $p \times p$ submatrix $\boldsymbol{A}_1(\theta)$ have full rank. Hence $\boldsymbol{A}_1(\theta)$ is invertible, and the rows of $\boldsymbol{A}_2(\theta)$ can be expressed as a linear combination of linearly independent rows of $\boldsymbol{A}_1(\theta)$; equivalently there is a $p \times (M-p)$ linear operator $\boldsymbol{P}_z$ between $\boldsymbol{A}_1(\theta)$ and $\boldsymbol{A}_2(\theta)$ [39, 45], i.e., $\boldsymbol{A}_2(\theta) = \boldsymbol{P}_z^H\boldsymbol{A}_1(\theta)$. Then $\boldsymbol{P}_z$ can be obtained from $\boldsymbol{R}_{z1}$ and $\boldsymbol{R}_{z2}$ in (8) as [39]

$$\boldsymbol{P}_z = (\boldsymbol{A}_1^H(\theta))^{-1}\boldsymbol{A}_2^H(\theta) = (\boldsymbol{R}_{z1}\boldsymbol{R}_{z1}^H)^{-1}\boldsymbol{R}_{z1}\boldsymbol{R}_{z2}^H. \quad (9)$$

Further by defining the matrix $\boldsymbol{Q}_z \triangleq [\boldsymbol{P}_z^T, -\boldsymbol{I}_{M-p}]^T$, in view of $\boldsymbol{A}(\theta) = [\boldsymbol{A}_1^T(\theta), \boldsymbol{A}_2^T(\theta)]^T$, we can get

$$\boldsymbol{Q}_z^H\boldsymbol{A}(\theta) = \boldsymbol{O}_{(M-p)\times p}. \quad (10)$$

Since the $M \times (M-p)$ matrix $\boldsymbol{Q}_z$ has full column rank equal to $M-p$, the columns of $\boldsymbol{Q}_z$ in fact form the basis for the null space $\mathcal{N}(\boldsymbol{A}(\theta))$ of $\boldsymbol{A}(\theta)$, and clearly the orthogonal projector onto the subspace spanned by the columns of $\boldsymbol{Q}_z$ is given by $\boldsymbol{\Pi}_z \triangleq \boldsymbol{Q}_z(\boldsymbol{Q}_z^H\boldsymbol{Q}_z)^{-1}\boldsymbol{Q}_z^H$, which implies that [39, 46]

$$\boldsymbol{\Pi}_z\boldsymbol{a}(\theta) = \boldsymbol{0}_{M\times 1}, \text{ for } \theta = \theta_k \quad (11)$$

where $\boldsymbol{a}(\theta) \triangleq [1, e^{j\alpha}, \cdots, e^{j(M-1)\alpha}]^T$. Evidently the orthogonal property (11) can be used to estimate the elevation angles $\{\theta_k\}_{k=1}^p$ in the SUMWE-like manner without any eigendecomposition.

Thus by using the orthogonal property in (11), when the number of snapshots is finite, the elevation angles $\{\theta_k\}_{k=1}^p$ can be estimated by minimizing the following cost function $f(\theta)$, i.e.,

$$\hat{\theta}_k = \arg\min_\theta f(\theta) \triangleq \arg\min_\theta \boldsymbol{a}^H(\theta)\hat{\boldsymbol{\Pi}}_z\boldsymbol{a}(\theta) \quad (12)$$

where

$$\hat{\boldsymbol{\Pi}}_z \triangleq \hat{\boldsymbol{Q}}_z(\hat{\boldsymbol{Q}}_z^H\hat{\boldsymbol{Q}}_z)^{-1}\hat{\boldsymbol{Q}}_z^H = \hat{\boldsymbol{Q}}_z(\boldsymbol{I}_{M-p} - \hat{\boldsymbol{P}}_z^H(\hat{\boldsymbol{P}}_z\hat{\boldsymbol{P}}_z^H + \boldsymbol{I}_p)^{-1}\hat{\boldsymbol{P}}_z)\hat{\boldsymbol{Q}}_z^H \quad (13)$$

$$\hat{\boldsymbol{P}}_z = (\hat{\boldsymbol{R}}_{z1}\hat{\boldsymbol{R}}_{z1}^H)^{-1}\hat{\boldsymbol{R}}_{z1}\hat{\boldsymbol{R}}_{z2}^H \quad (14)$$

and $\hat{\boldsymbol{Q}}_z = [\hat{\boldsymbol{P}}_z^T, -\boldsymbol{I}_{M-p}]^T$, in which $\hat{\boldsymbol{\Pi}}_z$ is calculated using the matrix inversion lemma implicitly [39], and the orthonormalization of the matrix $\hat{\boldsymbol{Q}}_z$ is used in $\hat{\boldsymbol{\Pi}}_z$ to improve the estimation performance [45].

REMARK 2 By considering the singular value decomposition (SVD) of matrix $\boldsymbol{A}(\theta)$, we readily verify that the orthogonal projector $\boldsymbol{\Pi}_z$ in (11) can be written as $\boldsymbol{\Pi}_z = \boldsymbol{I}_M - \boldsymbol{A}(\theta)(\boldsymbol{A}^H(\theta)\boldsymbol{A}(\theta))^{-1}\boldsymbol{A}^H(\theta)$ [39].

B. Estimation of Azimuth Angles with Automatic Pairing

Under the assumptions of the data model, from (2) and (4), we can form a new $(2M-p)\times 1$ combined signal vector received by the ULA along the x axis and the subarray $\bar{\boldsymbol{z}}_2(n)$ along the z axis as

$$\bar{\boldsymbol{y}}(n) \triangleq [\bar{\boldsymbol{z}}_2^T(n), \boldsymbol{x}^T(n)]^T = \overline{\boldsymbol{A}}(\theta,\phi)\boldsymbol{s}(n) + \bar{\boldsymbol{w}}_y(n) \quad (15)$$

where $\overline{\boldsymbol{A}}(\theta,\phi) \triangleq [\boldsymbol{A}_2^T(\theta), \boldsymbol{A}^T(\phi)]^T$ with columns $\bar{\boldsymbol{a}}(\theta_k,\phi_k) \triangleq [\boldsymbol{a}_2^T(\theta_k), \boldsymbol{a}^T(\phi_k)]^T$, and $\bar{\boldsymbol{w}}_y(n) \triangleq [\bar{\boldsymbol{w}}_{\bar{z}_2}^T(n), \boldsymbol{w}_x^T(n)]^T$. Then from (4) and (15), we easily obtain a $(2M-p)\times p$ cross-correlation matrix $\bar{\boldsymbol{R}}$ between the array data $\bar{\boldsymbol{y}}(n)$ and that received by the subarray $\bar{\boldsymbol{z}}_1(n)$ along the z axis as

$$\begin{aligned}\bar{\boldsymbol{R}} &\triangleq E\{\bar{\boldsymbol{y}}(n)\bar{\boldsymbol{z}}_1^H(n)\} = [\boldsymbol{R}_{\bar{z}_2\bar{z}_1}^T, \boldsymbol{R}_{\bar{z}_1 x}^*]^T \\ &= \overline{\boldsymbol{A}}(\theta,\phi)E\{\boldsymbol{s}(n)\boldsymbol{s}^H(n)\}\boldsymbol{A}_1^H(\theta) + E\{\bar{\boldsymbol{w}}_y(n)\boldsymbol{w}_{\bar{z}_1}^T(n)\} \\ &= \overline{\boldsymbol{A}}(\theta,\phi)\boldsymbol{R}_s\boldsymbol{A}_1^H(\theta) \end{aligned} \quad (16)$$

where $\boldsymbol{R}_{\bar{z}_2\bar{z}_1} \triangleq E\{\bar{\boldsymbol{z}}_2(n)\bar{\boldsymbol{z}}_1^H(n)\} = \boldsymbol{A}_2(\theta)\boldsymbol{R}_s\boldsymbol{A}_1^H(\theta)$. Clearly $\overline{\boldsymbol{R}}$ is not affected by the additive noises at these two ULAs. Under the basic assumptions, we easily find that the matrices $\boldsymbol{R}_s$ and $\boldsymbol{A}_1(\theta)$ are nonsingular and the matrix $\overline{\boldsymbol{A}}(\theta,\phi)$ has full column rank equal to p, and it follows from (16) that $\overline{\boldsymbol{R}}$ and $\overline{\boldsymbol{A}}(\theta,\phi)$ have the same range space, i.e., $\mathcal{R}(\overline{\boldsymbol{R}}) = \mathcal{R}(\overline{\boldsymbol{A}}(\theta,\phi))$, or equivalently,

$$\overline{\boldsymbol{\Pi}}\bar{\boldsymbol{a}}(\theta,\phi) = \boldsymbol{0}_{(2M-p)\times 1}, \quad \text{for } \theta=\theta_k \text{ and } \phi=\phi_k \quad (17)$$

where $k = 1, 2, \ldots, p$, and the projector $\overline{\boldsymbol{\Pi}}$ onto the null space $\mathcal{N}(\overline{\boldsymbol{R}})$(or $\mathcal{N}(\overline{\boldsymbol{A}}(\theta,\phi))$ of $\overline{\boldsymbol{R}}$(or $\overline{\boldsymbol{A}}(\theta,\phi)$) is given by (e.g., [47])

$$\overline{\boldsymbol{\Pi}} \triangleq \boldsymbol{I}_{2M-p} - \overline{\boldsymbol{R}}(\overline{\boldsymbol{R}}^H\overline{\boldsymbol{R}})^{-1}\overline{\boldsymbol{R}}^H. \quad (18)$$

Thus when the finite array data are available, from (17), we can estimate the pairs of the elevation and azimuth angles $\{\theta_k, \phi_k\}$ as

$$\{\hat{\theta}_k, \hat{\phi}_k\} = \arg\min_{\theta,\phi} f(\theta,\phi) \triangleq \arg\min_{\theta,\phi} \bar{\boldsymbol{a}}^H(\theta,\phi)\hat{\overline{\boldsymbol{\Pi}}}\bar{\boldsymbol{a}}(\theta,\phi). \quad (19)$$

Then by substituting the estimated elevation angles $\hat{\theta}_k$ obtained with (12) into $\bar{\boldsymbol{a}}(\theta,\phi)$ in (19), the azimuth angle ϕ_k can be estimated as

$$\hat{\phi}_k = \arg\min_{\phi} f_k(\phi) \triangleq \arg\min_{\phi} \bar{\boldsymbol{a}}^H(\phi)\boldsymbol{\Gamma}(\hat{\theta}_k)\bar{\boldsymbol{a}}(\phi) \quad (20)$$

where $\bar{\boldsymbol{a}}(\phi) \triangleq [1, \boldsymbol{a}^T(\phi)]^T$, and

$$\boldsymbol{\Gamma}(\hat{\theta}_k) \triangleq \boldsymbol{B}^H(\hat{\theta}_k)\hat{\overline{\boldsymbol{\Pi}}}\boldsymbol{B}(\hat{\theta}_k) = \begin{bmatrix} \boldsymbol{a}_2^H(\hat{\theta}_k)\hat{\overline{\boldsymbol{\Pi}}}_{11}\boldsymbol{a}_2(\hat{\theta}_k), & \boldsymbol{a}_2^H(\hat{\theta}_k)\hat{\overline{\boldsymbol{\Pi}}}_{12} \\ \hat{\overline{\boldsymbol{\Pi}}}_{21}\boldsymbol{a}_2(\hat{\theta}_k), & \hat{\overline{\boldsymbol{\Pi}}}_{22} \end{bmatrix} \quad (21)$$

while $\boldsymbol{B}(\theta) \triangleq \mathrm{diag}(\boldsymbol{a}_2(\theta), \boldsymbol{I}_M)$, $\hat{\overline{\boldsymbol{\Pi}}}_{ik}$ is the ikth block element of $\hat{\overline{\boldsymbol{\Pi}}}$ with compatible dimensions, and $\bar{\boldsymbol{a}}(\theta,\phi) = \boldsymbol{B}(\theta)\bar{\boldsymbol{a}}(\phi)$ is used implicitly. Obviously the estimated elevation angle $\hat{\theta}_k$ is paired with the estimated azimuth angle $\hat{\phi}_k$ automatically.

REMARK 3 By substituting (16) into (18), the orthogonal projection matrix $\overline{\boldsymbol{\Pi}}$ can be rewritten as $\overline{\boldsymbol{\Pi}} = \boldsymbol{I}_{2M-p} - \overline{\boldsymbol{A}}(\theta,\phi)(\overline{\boldsymbol{A}}^H(\theta,\phi)\overline{\boldsymbol{A}}(\theta,\phi))^{-1}\overline{\boldsymbol{A}}^H(\theta,\phi)$, where the ikth block element is given by

$$\overline{\boldsymbol{\Pi}}_{11} \triangleq I_{M-p} - \boldsymbol{A}_2(\theta)(\overline{\boldsymbol{A}}^H(\theta,\phi)\overline{\boldsymbol{A}}(\theta,\phi))^{-1}\boldsymbol{A}_2^H(\theta) \quad (22)$$

$$\overline{\boldsymbol{\Pi}}_{12} \triangleq -\boldsymbol{A}_2(\theta)(\overline{\boldsymbol{A}}^H(\theta,\phi)\overline{\boldsymbol{A}}(\theta,\phi))^{-1}\boldsymbol{A}^H(\phi) \quad (23)$$

$$\overline{\boldsymbol{\Pi}}_{21} \triangleq -\boldsymbol{A}(\phi)(\overline{\boldsymbol{A}}^H(\theta,\phi)\overline{\boldsymbol{A}}(\theta,\phi))^{-1}\boldsymbol{A}_2^H(\theta) \quad (24)$$

$$\overline{\boldsymbol{\Pi}}_{22} \triangleq I_M - \boldsymbol{A}(\phi)(\overline{\boldsymbol{A}}^H(\theta,\phi)\overline{\boldsymbol{A}}(\theta,\phi))^{-1}\boldsymbol{A}^H(\phi). \quad (25)$$

C. Modified Estimation of Azimuth Angles

Although the estimated azimuth angle $\hat{\phi}_k$ can be paired correctly with the elevation angle $\hat{\theta}_k$ by using (20), the finite number of snapshots and/or low SNR may cause these estimates $\hat{\theta}_k$ and $\hat{\phi}_k$ outside the permissible region shown in Fig. 2(a), i.e., the estimation failure occurs in this situation. Hence a measure should be taken to alleviate the problem of estimation failure.

By considering the geometry restrictions in (3) for the parameters θ_k and ϕ_k, from (20), we can estimate the azimuth angle ϕ_k for the estimated elevation angle $\hat{\theta}_k$ as

$$\hat{\phi}_k = \arg\min_{\phi} \bar{\boldsymbol{a}}^H(\phi)\boldsymbol{\Gamma}(\hat{\theta}_k)\bar{\boldsymbol{a}}(\phi) \quad \text{subject to} \quad (26)$$

$$\begin{cases} -\hat{\theta}_k + 90^\circ \le \phi_k \le \hat{\theta}_k + 90^\circ, \text{ for } 0^\circ \le \hat{\theta}_k \le 90^\circ \\ \hat{\theta}_k - 90^\circ \le \phi_k \le -\hat{\theta}_k + 270^\circ, \text{ for } 90^\circ \le \hat{\theta}_k \le 180^\circ \end{cases}$$

where the estimated elevation angles $\{\hat{\theta}_k\}_{k=1}^p$ are obtained with (12). Evidently the estimates $\hat{\theta}_k$ and $\hat{\phi}_k$ have a one-to-one relationship without the need of the pair-matching procedure, and they are ensured to lie in the permissible region to overcome the estimation failure.

D. Implementation of Batch Method for 2-D DOA Estimation

When N snapshots of array data $\{\boldsymbol{x}(n), \boldsymbol{z}(n)\}_{n=1}^{N}$ are available, from (12) and (26), the implementation of the proposed CODEC method can be summarized as follows.

1) Calculate the estimates of the cross-correlation matrices $\boldsymbol{R}_{zx}$ in (5) and $\boldsymbol{R}_{\bar{z}_2\bar{z}_1}$ in (16) as

$$\widehat{\boldsymbol{R}}_{zx} = \frac{1}{N}\sum_{n=1}^{N} \boldsymbol{z}(n)\boldsymbol{x}^H(n) \tag{27}$$

$$\widehat{\boldsymbol{R}}_{\bar{z}_2\bar{z}_1} = \frac{1}{N}\sum_{n=1}^{N} \bar{\boldsymbol{z}}_2(n)\bar{\boldsymbol{z}}_1^H(n). \tag{28}$$

$8M^2N + 8(M-p)pN$ flops.

2) Form the estimates of the cross-correlation matrices $\boldsymbol{R}_z$ in (8) and $\overline{\boldsymbol{R}}$ in (16) from $\widehat{\boldsymbol{R}}_{zx}$ and $\widehat{\boldsymbol{R}}_{\bar{z}_2\bar{z}_1}$ as $\widehat{\boldsymbol{R}}_z = [\widehat{\boldsymbol{R}}_{zx}, \boldsymbol{J}_M\widehat{\boldsymbol{R}}_{zx}^*]$ and $\widehat{\overline{\boldsymbol{R}}} = [\widehat{\boldsymbol{R}}_{\bar{z}_2\bar{z}_1}^T, \widehat{\boldsymbol{R}}_{\bar{z}_1x}^*]^T$, where $\widehat{\boldsymbol{R}}_{\bar{z}_1x}$ is the submatrix consisting of the first p rows of $\widehat{\boldsymbol{R}}_{zx}$ in (27).

3) Calculate the estimated orthogonal projectors $\widehat{\boldsymbol{\Pi}}_z$ by using (13) and (14) and $\widehat{\overline{\boldsymbol{\Pi}}}$ by using (18).

$$16Mp^2 + 16Mp(M-p) + 24p^2(M-p) + 8(M+p) \times (M-p)^2 + 8M^2(M-p) + 2p^2 + 2(M-p)^2 + 16p^2(2M-p) + 8(2M-p)^2p + O(p^3) \text{ flops}$$

4) Estimate the elevation angles $\{\theta_k\}$ by finding the phases of the p zeros of the polynomial $p_\theta(z)$ closest to the unit circle in the z–plane with (12), where $p_\theta(z) \triangleq z^{M-1}\boldsymbol{p}_\theta^H(z)\widehat{\boldsymbol{\Pi}}_z\boldsymbol{p}_\theta(z)$, $\boldsymbol{p}_\theta(z) \triangleq [1, z, \cdots, z^{M-1}]^T$, and $z \triangleq e^{j2\pi d\cos\theta/\lambda}$.

$$(M-1)^2 + \mathcal{C}_\theta \text{ flops}$$

5) Calculate the matrix $\boldsymbol{\Gamma}(\hat{\theta}_k)$ in (21) with (18), and estimate the azimuth angle ϕ_k by finding the phase of the zero of the polynomial $p_{\phi_k}(z)$ satisfying the constraint given in (26) and closest to the unit circle in the z–plane for $k = 1, 2, \ldots, p$, where $p_{\phi_k}(z) \triangleq z^M\boldsymbol{p}_\phi^H(z)\boldsymbol{\Gamma}(\hat{\theta}_k)\boldsymbol{p}_\phi(z)$, $\boldsymbol{p}_\phi(z) \triangleq [1, z, \cdots, z^M]^T$, and $z \triangleq e^{j2\pi d\cos\phi/\lambda}$.

$$p(8(M-p) + 8(M-p)^2 + 16M(M-p) + M^2 + \mathcal{C}_\phi) \text{ flops}$$

In the above implementation, the computational complexity of each step is roughly indicated in terms of the number of MATLAB flops. Consequently we can find that the computational complexity of the CODEC method is nearly $8M^2N + 16M^3$ flops, which is less than that of the CODE method [40] (i.e., $32M^2N + 160M^3 + 4M^2p^2$ flops), when $M \gg p$, which occurs often in application of DOA estimation.

REMARK 4 Certainly we have the spectral approach version of the CODEC method to estimate the elevation and azimuth angles by searching the p highest peaks of spatial spectrum $P(\theta) = 1/\boldsymbol{a}^H(\theta)\widehat{\boldsymbol{\Pi}}_z\boldsymbol{a}(\theta)$ and the highest peak of spectrum $P(\phi_k) = 1/\bar{\boldsymbol{a}}^H(\phi)\boldsymbol{\Gamma}(\hat{\theta}_k)\bar{\boldsymbol{a}}(\phi)$ for $k = 1, 2, \ldots, p$. However, the 1-D spectral searching is rather a computationally brute-force procedure, where a high density search grid is required, and it is affected by the radial estimation errors [2, 48]. Hence in the above implementation, the needs for the exhaustive spectral search are eliminated by using the search-free 1-D polynomial rooting. Note that various computationally efficient algorithms have been explored for polynomial root finding with different computational complexity in the literature (cf., e.g. [49–51]). Consequently for example, when the Lindsey-Fox algorithm for root finding [51] is employed, the complexities of polynomial rooting in steps 4 and 5 can be approximated as $\mathcal{C}_\theta = O((2M-1)^2)$ and $\mathcal{C}_\phi = O((2M+1)^2)$ flops, and they are less than that the ordinary MATLAB function roots, which requires the calculation of the eigenvalues of an associated coefficient companion matrix (e.g., [52]).

IV. ON-LINE ALGORITHM FOR 2-D DOA TRACKING

Now we consider the on-line implementation of the batch CODEC method described above for estimating the time-varying elevation and azimuth angles of multiple moving targets with crossover points on their trajectories. Here we assume that $(\theta_k(n), \phi_k(n))$ are slowly time varying so that $\theta_k(\bar{n}N_s+1) \approx \theta_k(\bar{n}N_s+2) \approx \cdots \approx \theta_k((\bar{n}+1)N_s)$ and $\phi_k(\bar{n}N_s+1) \approx \phi_k(\bar{n}N_s+2) \approx \cdots \approx \phi_k((\bar{n}+1)N_s)$ for $n \in (\bar{n}N_s, (\bar{n}+1)N_s]$ and $\bar{n} = 0, 1, \cdots$, where there are N_s snapshots of array data available for DOA updating (cf. [16, 19] and references therein). Then by denoting $\theta_k(\bar{n}N_s)$ and $\phi_k(\bar{n}N_s))$ as $\theta_k(\bar{n})$ and $\phi_k(\bar{n})$, the 2-D DOA tracking can be formulated as the estimation of the elevation-azimuth pairs $\{(\theta_k(\bar{n}), \phi_k(\bar{n}))\}$ from N_s snapshots of $\{\boldsymbol{z}(n), \boldsymbol{x}(n)\}$ measured at $n = \bar{n}N_s+1, \bar{n}N_s+2, \cdots, (\bar{n}+1)N_s$ while maintaining the correct association between the current estimates $(\hat{\theta}_k(\bar{n}), \hat{\phi}_k(\bar{n}))$ and the previous estimates $(\hat{\theta}_k(\bar{n}-1), \hat{\phi}_k(\bar{n}-1))$ for the same incident signal.

A. Luenberger Observer Based State Estimation

Similar to the previously proposed 1-D DOA tracking [19], where the Luenberger observer [41] with a deterministic dynamic state model of the direction trajectory was employed to solve the association problem of the estimated directions at two successive time instants and to eliminate the estimation of the unknown variances of additive process and measurement noises required by the Kalman filtering, here we consider the problem of 2-D DOA tracking by using the Luenberger observer. By letting the bearing velocities and accelerations of $\theta_k(\bar{n})$(or $\phi_k(\bar{n})$) at the instant $\bar{n}$ be $\dot{\theta}_k(\bar{n})$(or $\dot{\phi}_k(n)$) and $\ddot{\theta}_k(\bar{n})$(or $\ddot{\phi}_k(\bar{n})$) and denoting the state vectors of the dynamic models for the elevation and azimuth angles as $\boldsymbol{\zeta}_{\theta_k}(\bar{n}) \triangleq [\theta_k(\bar{n}), \dot{\theta}_k(\bar{n}), \ddot{\theta}_k(\bar{n})]^T$ and $\boldsymbol{\zeta}_{\phi_k}(\bar{n}) \triangleq [\phi_k(\bar{n}), \dot{\phi}_k(\bar{n}), \ddot{\phi}_k(\bar{n})]^T$, the slowly time-varying

trajectories of angles $\theta_k(\bar{n})$ and $\phi_k(\bar{n})$ can be approximately expressed by a deterministic state model with constant acceleration in the absence of process and measurement noises and the 2-D DOAs can be measured from the corresponding state vectors

$$\boldsymbol{\zeta}_{\theta_k}(\bar{n}) = \boldsymbol{F}\boldsymbol{\zeta}_{\theta_k}(\bar{n}-1), \quad \theta_k(\bar{n}) = \boldsymbol{c}^T\boldsymbol{\zeta}_{\theta_k}(\bar{n}) \tag{29}$$

$$\boldsymbol{\zeta}_{\phi_k}(\bar{n}) = \boldsymbol{F}\boldsymbol{\zeta}_{\phi_k}(\bar{n}-1), \quad \phi_k(\bar{n}) = \boldsymbol{c}^T\boldsymbol{\zeta}_{\phi_k}(\bar{n}) \tag{30}$$

where $\boldsymbol{F}$ and $\boldsymbol{c}$ are the transition matrix and measurement vector given by $\boldsymbol{F} \triangleq [1, N_s, 0.5N_s^2; 0, 1, N_s; 0, 0, 1]$ and $\boldsymbol{c} \triangleq [1, 0, 0]^T$ (see, e.g., [1, 16, 19]).

Then by using the measurements $\theta_k(\bar{n})$ and $\phi_k(\bar{n})$, the Luenberger current observers for estimation of the azimuth and elevation angles at the instant $\bar{n}$ are given by (cf. [53] and references therein)

$$\widehat{\boldsymbol{\zeta}}_{\theta_k}(\bar{n}) = \overline{\zeta}_{\theta_k}(\bar{n}) + \boldsymbol{g}_{\theta_k}(\theta_k(\bar{n}) - \boldsymbol{c}^T\overline{\boldsymbol{\zeta}}_{\theta_k}(\bar{n})) \tag{31}$$

$$\overline{\boldsymbol{\zeta}}_{\theta_k}(\bar{n}) = \boldsymbol{F}\widehat{\boldsymbol{\zeta}}_{\theta_k}(\bar{n}-1) \tag{32}$$

$$\hat{\theta}_k(\bar{n}) = \boldsymbol{c}^T\widehat{\boldsymbol{\zeta}}_{\theta_k}(\bar{n}) \tag{33}$$

$$\widehat{\boldsymbol{\zeta}}_{\phi_k}(\bar{n}) = \overline{\boldsymbol{\zeta}}_{\phi_k}(\bar{n}) + \boldsymbol{g}_{\phi_k}(\phi_k(\bar{n}) - \boldsymbol{c}^T\overline{\boldsymbol{\zeta}}_{\phi_k}(\bar{n})) \tag{34}$$

$$\overline{\boldsymbol{\zeta}}_{\phi_k}(\bar{n}) = \boldsymbol{F}\widehat{\boldsymbol{\zeta}}_{\phi_k}(\bar{n}-1) \tag{35}$$

$$\hat{\phi}_k(\bar{n}) = \boldsymbol{c}^T\widehat{\boldsymbol{\zeta}}_{\phi_k}(\bar{n}) \tag{36}$$

where $\widehat{\boldsymbol{\zeta}}_{\theta_k}(\bar{n})$(or $\widehat{\boldsymbol{\zeta}}_{\phi_k}(\bar{n})$) is the current estimate based on the measurement $\theta_k(\bar{n})$(or $\phi_k(\bar{n})$) at the current instant $\bar{n}$, while $\overline{\boldsymbol{\zeta}}_{\theta_k}(\bar{n})$(or $\overline{\boldsymbol{\zeta}}_{\phi_k}(\bar{n})$) is the predicted estimate based on a model prediction from the estimate obtained at the previous instant $\bar{n}-1$, and $\boldsymbol{g}_{\theta_k}$ and $\boldsymbol{g}_{\phi_k}$ are the observer gains, which should be chosen appropriately to ensure the magnitudes of all eigenvalues of the matrices $\boldsymbol{F} - \boldsymbol{g}_{\theta_k}\boldsymbol{c}^T\boldsymbol{F}$ and $\boldsymbol{F} - \boldsymbol{g}_{\phi_k}\boldsymbol{c}^T\boldsymbol{F}$ be strictly less than one so that the observers in (31)–(36) are asymptotically stable for any initial values of $\widehat{\boldsymbol{\zeta}}_{\theta_k}(0)$ and $\widehat{\boldsymbol{\zeta}}_{\phi_k}(0)$.

REMARK 5 Different from the Luenberger prediction estimator used in [19], in order to improve the response of the estimator, which is about a cycle faster, herein an alternative Luenberger state observer (i.e., current estimator) is employed by using the information of the current measurement. Additionally the desired poles of these observer gains can be designed as one pair of conjugate complex poles and one real pole within the unit circle in the z-plane (see Appendix A for details).

B. Tracking of Crossing Angles

In fact, the measurements $\theta_k(\bar{n})$ and $\phi_k(\bar{n})$ and the state vectors $\widehat{\boldsymbol{\zeta}}_{\theta_k}(\bar{n})$ and $\widehat{\boldsymbol{\zeta}}_{\phi_k}(\bar{n})$ in (31) and (34) are unknown and should be estimated from the available array data by exploiting the batch CODEC method and Luenberger observer described above. During the interval of direction updating $(\bar{n}T, (\bar{n}+1)T]$ (i.e, $n = \bar{n}N_s + 1, \bar{n}N_s + 2, \cdots, (\bar{n}+1)N_s$), the instantaneous estimates of the cross-correlation matrices $\boldsymbol{R}_{zx}$ in (5) and $\boldsymbol{R}_{\bar{z}_2\bar{z}_1}$ in (16) (i.e., (27) and (28)) can be recursively computed by rank-1 updating as

$$\widehat{\boldsymbol{R}}_{zx}(n) = \bar{\gamma}\widehat{\boldsymbol{R}}_{zx}(n-1) + \boldsymbol{z}(n)\boldsymbol{x}^H(n) \tag{37}$$

$$\widehat{\boldsymbol{R}}_{\bar{z}_2\bar{z}_1}(n) = \bar{\gamma}\widehat{\boldsymbol{R}}_{\bar{z}_2\bar{z}_1}(n-1) + \bar{\boldsymbol{z}}_2(n)\bar{\boldsymbol{z}}_1^H(n) \tag{38}$$

where $\bar{\gamma}$ is the forgetting factor given by $0 < \bar{\gamma} < 1$, which should be selected appropriately to accommodate for the time-variations of azimuth and elevation angles and usually chosen close to one for achieving good tracking performance and reducing the sensitivity to additive noise. When $n = (\bar{n}+1)N_s$, by forming the instantaneous estimates $\widehat{\boldsymbol{R}}_z(n)$ and $\widehat{\overline{\boldsymbol{R}}}(n)$ of the cross-correlation matrices $\boldsymbol{R}_z$ in (8) and $\overline{\boldsymbol{R}}$ in (16) from (37) and (38), we can obtain the instantaneous orthogonal projectors $\widehat{\boldsymbol{\Pi}}_z(n)$ with (13) and (14) and $\widehat{\overline{\boldsymbol{\Pi}}}(n)$ with (18), which are denoted as $\widehat{\boldsymbol{\Pi}}_z(\bar{n})$ and $\widehat{\overline{\boldsymbol{\Pi}}}(\bar{n})$. Then by considering the Taylor series expansion of $f(\theta)$ in (12) and using the instantaneous orthogonal projector $\widehat{\boldsymbol{\Pi}}_z(\bar{n})$ and a predicated state vectors $\widehat{\boldsymbol{\zeta}}_{\theta_k}(\bar{n}|\bar{n}-1)$ (i.e., $\hat{\theta}_k(\bar{n}|\bar{n}-1)$), the "measurement" $\tilde{\theta}_k(\bar{n})$ of elevation angle $\theta_k(\bar{n})$ in (31) can be estimated with the approximate Newton iteration as

$$\tilde{\theta}_k(\bar{n}) = \hat{\theta}_k(\bar{n}|\bar{n}-1) - \left.\frac{\mathrm{Re}\{\boldsymbol{d}^H(\theta)\widehat{\boldsymbol{\Pi}}_z(\bar{n})\boldsymbol{a}(\theta)\}}{\boldsymbol{d}^H(\theta)\widehat{\boldsymbol{\Pi}}_z(\bar{n})\boldsymbol{d}(\theta)}\right|_{\theta=\hat{\theta}_k(\bar{n}|\bar{n}-1)} \tag{39}$$

where $\boldsymbol{d}(\theta) \triangleq d(\boldsymbol{a}(\theta))/d\theta = j(2\pi d\sin\theta/\lambda)[0, e^{j\alpha}, \cdots, (M-1)e^{j(M-1)\alpha}]^T$, while the state vector $\widehat{\boldsymbol{\zeta}}_{\theta_k}(\bar{n})$ in (31) can be estimated by refining the predicated state vector $\widehat{\boldsymbol{\zeta}}_{\theta_k}(\bar{n}|\bar{n}-1)$ as

$$\widehat{\boldsymbol{\zeta}}_{\theta_k}(\bar{n}|\bar{n}) = \widehat{\boldsymbol{\zeta}}_{\theta_k}(\bar{n}|\bar{n}-1) + \boldsymbol{g}_{\theta_k}(\tilde{\theta}_k(\bar{n}) - \hat{\theta}_k(\bar{n}|\bar{n}-1)) \tag{40}$$

and hence the elevation angle $\theta_k(\bar{n})$ can be estimated as

$$\hat{\theta}_k(\bar{n}) = c^T\widehat{\boldsymbol{\zeta}}_{\theta_k}(\bar{n}|\bar{n}). \tag{41}$$

In a similar way, by using the instantaneous orthogonal projector $\widehat{\overline{\boldsymbol{\Pi}}}(\bar{n})$ and a predicated state vector $\widehat{\boldsymbol{\zeta}}_{\phi_k}(\bar{n}|\bar{n}-1)$ (i.e., $\hat{\phi}_k(\bar{n}|\bar{n}-1)$) and substituting the estimate $\hat{\theta}_k(\bar{n})$ in (41) into (21), from (20), we can obtain the measurement $\tilde{\phi}_k(\bar{n})$ of azimuth angle $\phi_k(\bar{n})$ in (34) by the following approximate Newton iteration

$$\tilde{\phi}_k(\bar{n}) = \hat{\phi}_k(\bar{n}|\bar{n}-1) - \left.\frac{\mathrm{Re}\{\overline{\boldsymbol{d}}^H(\phi)\boldsymbol{\Gamma}(\hat{\theta}_k(\bar{n}))\bar{\boldsymbol{a}}(\phi)\}}{\overline{\boldsymbol{d}}^H(\phi)\boldsymbol{\Gamma}(\hat{\theta}_k(\bar{n}))\bar{\boldsymbol{d}}(\phi)}\right|_{\phi=\hat{\phi}_k(\bar{n}|\bar{n}-1)} \tag{42}$$

where $\overline{\boldsymbol{d}}(\phi) \triangleq d(\bar{\boldsymbol{a}}(\phi))/d\phi = j(2\pi d\sin\phi/\lambda)[0, e^{j\beta}, \cdots, Me^{jM\beta}]^T$. Then by using this measurement in (42), we can get the state vector $\widehat{\boldsymbol{\zeta}}_{\phi_k}(\bar{n})$ in (34) by refining the predicated state vector $\widehat{\boldsymbol{\zeta}}_{\phi_k}(\bar{n}|\bar{n}-1)$ as

$$\widehat{\boldsymbol{\zeta}}_{\phi_k}(\bar{n}|\bar{n}) = \widehat{\boldsymbol{\zeta}}_{\phi_k}(\bar{n}|\bar{n}-1) + \boldsymbol{g}_{\phi_k}(\tilde{\phi}_k(\bar{n}) - \hat{\phi}_k(\bar{n}|\bar{n}-1)) \tag{43}$$

and thus the azimuth angle $\phi_k(\bar{n})$ can be estimated as

$$\hat{\phi}_k(\bar{n}) = c^T\widehat{\boldsymbol{\zeta}}_{\phi_k}(\bar{n}|\bar{n}). \tag{44}$$

C. On-line Algorithm for 2-D DOA Tracking

Therefore based on the batch CODEC method and Luenberger observer described above, we have the following on-line algorithm for tracking 2-D DOAs of multiple moving targets.

1) Estimate the initial values of $\theta_k(\bar{n})$ and $\phi_k(\bar{n})$ from the N_s snapshots of $\{\boldsymbol{z}(n), \boldsymbol{x}(n)\}_{n=1}^{N_s}$ with the batch CODEC method described in Section III-D, and denote them as $\hat{\theta}_k(0|0)$ and $\hat{\phi}_k(0|0)$.

2) Initialize the Luenberger observers by $\widehat{\boldsymbol{\zeta}}_{\theta_k}(0|0)=[\hat{\theta}_k(0|0), 0, 0]^T$ and $\widehat{\boldsymbol{\zeta}}_{\phi_k}(0|0)=[\hat{\phi}_k(0|0), 0, 0]^T$, and set the instantaneous cross-correlation matrices $\widehat{\boldsymbol{R}}_{zx}(N_s) = \boldsymbol{O}_{M\times M}$ and $\widehat{\boldsymbol{R}}_{\bar{z}_2\bar{z}_1}(N_s) = \boldsymbol{O}_{(M-p)\times p}$, while updating the instant index to $\bar{n} = 1$ and $n = \bar{n}N_s + 1$.

3) Calculate the predicated state vectors $\widehat{\boldsymbol{\zeta}}_{\theta_k}(\bar{n}|\bar{n}-1)$ and $\widehat{\boldsymbol{\zeta}}_{\phi_k}(\bar{n}|\bar{n}-1)$ and predicated angles $\hat{\theta}_k(\bar{n}|\bar{n}-1)$ and $\hat{\phi}_k(\bar{n}|\bar{n}-1)$ from the existing estimated state vectors $\widehat{\boldsymbol{\zeta}}_{\theta_k}(\bar{n}-1|\bar{n}-1)$ and $\widehat{\boldsymbol{\zeta}}_{\phi_k}(\bar{n}-1|\bar{n}-1)$ with Luenberger observers with (32), (33), (35), and (36) as

$$\widehat{\boldsymbol{\zeta}}_{\theta_k}(\bar{n}|\bar{n}-1) = \boldsymbol{F}\widehat{\boldsymbol{\zeta}}_{\theta_k}(\bar{n}-1|\bar{n}-1) \tag{45}$$

$$\widehat{\boldsymbol{\zeta}}_{\phi_k}(\bar{n}|\bar{n}-1) = \boldsymbol{F}\widehat{\boldsymbol{\zeta}}_{\phi_k}(\bar{n}-1|\bar{n}-1) \tag{46}$$

$$\hat{\theta}_k(\bar{n}|\bar{n}-1) = \boldsymbol{c}^T\widehat{\boldsymbol{\zeta}}_{\theta_k}(\bar{n}|\bar{n}-1) \tag{47}$$

$$\hat{\phi}_k(\bar{n}|\bar{n}-1) = \boldsymbol{c}^T\widehat{\boldsymbol{\zeta}}_{\phi_k}(\bar{n}|\bar{n}-1). \tag{48}$$

4) Estimate the instantaneous cross-correlation matrices $\widehat{\boldsymbol{R}}_{zx}(n)$ and $\widehat{\boldsymbol{R}}_{\bar{z}_2\bar{z}_1}(n)$ with (37) and (38).

5) If $n = (\bar{n}+1)N_s$, go to the next step; otherwise update the instant index as $n = n + 1$, and return to step 4.

6) Calculate the estimated orthogonal projectors $\widehat{\boldsymbol{\Pi}}_z(\bar{n})$ with (13) and (14) and $\widehat{\overline{\boldsymbol{\Pi}}}(\bar{n})$ with (18).

7) Calculate the measurement $\tilde{\theta}_k(\bar{n})$ by using the projector $\widehat{\boldsymbol{\Pi}}_z(\bar{n})$ and the predicted angle $\hat{\theta}_k(\bar{n}|\bar{n}-1)$ with (39), and estimate the elevation angles $\hat{\theta}_k(\bar{n})$ with (40) and (41) for $k = 1, 2, \ldots, p$.

8) Calculate the matrix $\boldsymbol{\Gamma}(\hat{\theta}_k(\bar{n}))$ in (42) with (21) by using $\hat{\theta}_k(\bar{n})$ and $\widehat{\overline{\boldsymbol{\Pi}}}(\bar{n})$, and estimate the measurement $\tilde{\phi}_k(\bar{n})$ by using the predicted angle $\hat{\phi}_k(\bar{n}|\bar{n}-1)$ with (42).

9) Calculate the refined state vector $\widehat{\boldsymbol{\zeta}}_{\phi_k}(\bar{n}|\bar{n})$ and estimate the azimuth angle $\hat{\phi}_k(\bar{n})$ with (43) and (44).

10) Update the instant index of angle updating as $\bar{n} = \bar{n} + 1$ and $n = \bar{n}N_s + 1$, and go to step 3.

REMARK 6 The Luenberger observer plays important roles of refining (or smoothing) the measured elevation and azimuth angles $\tilde{\theta}_k(\bar{n})$ and $\tilde{\phi}_k(\bar{n})$ obtained from the array data and maintaining the association between the estimates $\{(\hat{\theta}_k(\bar{n}), \hat{\phi}_k(\bar{n}))\}$ at different time instants of angle updating.

V. PERFORMANCE ANALYSIS OF CODEC METHOD

Here we analyze the statistical properties of the proposed batch CODEC method with (12) and (20) for a large number of snapshots. When the number of snapshots N is sufficiently large, we can find that the estimated elevation angle $\hat{\theta}_k$ obtained by minimizing the cost function (12) and the estimated azimuth angle $\hat{\phi}_k$ by minimizing the cost function (20) approach the true parameters θ_k and ϕ_k with probability one (cf. [39, Appendix A]).

By defining the following notations for convenience of formulation as $H_{zkk} \triangleq \boldsymbol{d}^H(\theta_k)\boldsymbol{\Pi}_z d(\theta_k)$, $\boldsymbol{h}(\theta_k) \triangleq \boldsymbol{R}_{\bar{z}_1x}^H(\boldsymbol{R}_{z_1}\boldsymbol{R}_{z_1}^H)^{-1}\boldsymbol{a}_1(\theta_k)$, $\overline{\boldsymbol{h}}(\theta_k) \triangleq \widetilde{\boldsymbol{R}}_{\bar{z}_1x}^H(\boldsymbol{R}_{z1}\boldsymbol{R}_{z1}^H)^{-1}\boldsymbol{a}_1(\theta_k)$, $\bar{H}_{kk} \triangleq \mathrm{Re}\{\boldsymbol{d}^H(\phi_k)\boldsymbol{A}(\phi)(\overline{\boldsymbol{A}}^H(\theta,\phi)\cdot\overline{\boldsymbol{A}}(\theta,\phi))^{-1}\boldsymbol{A}_2^H(\theta)\boldsymbol{d}_2(\theta_k)\}$, $\tilde{H}_{kk} \triangleq \boldsymbol{d}^H(\phi_k)\overline{\boldsymbol{\Pi}}_{22}\boldsymbol{d}(\phi_k)$, $\boldsymbol{g}(\theta_k) \triangleq \boldsymbol{\Pi}_z\boldsymbol{d}(\theta_k)$, $\bar{g}(\theta_k,\phi_k) \triangleq [\overline{\boldsymbol{\Pi}}_{12}^T, \overline{\boldsymbol{\Pi}}_{22}^T]^T\boldsymbol{d}(\phi_k)$, $\boldsymbol{b}(\theta_k,\phi_k) \triangleq (\boldsymbol{R}_s\boldsymbol{A}_1^H(\theta))^{-1}\boldsymbol{e}_k$, $\boldsymbol{\Gamma} \triangleq [\boldsymbol{O}_{M\times(M-p)}, \boldsymbol{I}_M]^T$, $\overline{\boldsymbol{\Gamma}} \triangleq [\boldsymbol{I}_p, \boldsymbol{O}_{p\times(M-p)}]^T$, $\widetilde{\boldsymbol{\Gamma}} \triangleq [\boldsymbol{O}_{(2M-p)\times M}, [\boldsymbol{I}_{M-p}, \boldsymbol{O}_{(M-p)\times M}]^T]$, where $\boldsymbol{d}(\theta_k) \triangleq d(\boldsymbol{a}(\theta))/(d\theta)|_{\theta=\theta_k}$, $\boldsymbol{d}(\phi_k) \triangleq d(\boldsymbol{a}(\phi))/(d\phi)|_{\phi=\phi_k}$, $\boldsymbol{d}_2(\theta_k) \triangleq d(\boldsymbol{a}_2(\theta))/(d\theta)|_{\theta=\theta_k}$, $\boldsymbol{e}_k$ is a $p\times 1$ unit vector with a unity element at the kth location and zeros elsewhere, we obtain the asymptotic (large-sample) MSE expressions of $\hat{\theta}_k$ and $\hat{\phi}_k$ as follows.

THEOREM 1 *For the estimates $\hat{\theta}_k$ and $\hat{\phi}_k$ obtained by minimizing the cost functions $f(\theta)$ in (12) and $f_k(\phi)$ in (20), the large-sample MSEs of these estimates are given by*

$$\begin{aligned}\mathrm{MSE}(\hat{\theta}_k) &\triangleq E\{(\hat{\theta}_k-\theta_k)^2\}\\ &= \frac{\sigma^2}{2N\bar{H}_{zkk}^2}\mathrm{Re}\{H_{zkk}\boldsymbol{h}^H(\theta_k)\boldsymbol{R}_{xx}\boldsymbol{h}(\theta_k)\\ &\quad + 2\boldsymbol{g}^H(\theta_k)\boldsymbol{J}_M\boldsymbol{g}^*(\theta_k)\overline{\boldsymbol{h}}^T(\theta_k)\boldsymbol{R}_{xx}\boldsymbol{h}(\theta_k)\\ &\quad + H_{zkk}\overline{\boldsymbol{h}}^T(\theta_k)\boldsymbol{R}_{xx}\overline{\boldsymbol{h}}^*(\theta_k)\}\end{aligned} \tag{49}$$

$$\begin{aligned}\mathrm{MSE}(\hat{\phi}_k) &\triangleq E\{(\hat{\phi}_k-\phi_k)^2\}\\ &= \frac{\bar{H}_{kk}^2}{\tilde{H}_{kk}^2}\mathrm{MSE}(\hat{\theta}_k)\\ &\quad + \frac{\sigma^2}{2N\tilde{H}_{kk}}\mathrm{Re}\{\boldsymbol{b}^H(\theta_k,\phi_k)\boldsymbol{R}_{\bar{z}_1\bar{z}_1}\boldsymbol{b}(\theta_k,\phi_k)\}\\ &\quad + \frac{\sigma^2\bar{H}_{kk}}{N\tilde{H}_{kk}^2H_{zkk}}\mathrm{Re}\{\sigma^2\overline{\boldsymbol{g}}^H(\theta_k,\phi_k)\\ &\quad \times\boldsymbol{\Gamma}\boldsymbol{h}(\theta_k)\boldsymbol{g}^H(\theta_k)\overline{\boldsymbol{\Gamma}}\boldsymbol{b}(\theta_k,\phi_k)\\ &\quad + \bar{\boldsymbol{g}}^H(\theta_k,\phi_k)\widetilde{\boldsymbol{\Gamma}}\boldsymbol{J}_M\boldsymbol{g}^*(\theta_k)\overline{\boldsymbol{h}}^T(\theta_k)\boldsymbol{R}_{\bar{z}_1x}^H\boldsymbol{b}(\theta_k,\phi_k)\\ &\quad + \bar{\boldsymbol{g}}^H(\theta_k,\phi_k)\widetilde{\boldsymbol{\Gamma}}\boldsymbol{g}(\theta_k)\boldsymbol{h}^H(\theta_k)\boldsymbol{R}_{\bar{z}_1x}^H\boldsymbol{b}(\theta_k,\phi_k)\\ &\quad + \sigma^2\bar{\boldsymbol{g}}^H(\theta_k,\phi_k)\boldsymbol{\Gamma}\overline{\boldsymbol{h}}^*(\theta_k)\boldsymbol{g}^T(\theta_k)\boldsymbol{J}_M\overline{\boldsymbol{\Gamma}}\boldsymbol{b}(\theta_k,\phi_k)\}\end{aligned} \tag{50}$$

where $\boldsymbol{R}_{xx} \triangleq E\{\boldsymbol{x}(n)\boldsymbol{x}^H(n)\} = \boldsymbol{A}(\phi)\boldsymbol{R}_s\boldsymbol{A}^H(\phi) + \sigma^2\boldsymbol{I}_M$ and $\boldsymbol{R}_{\bar{z}_1\bar{z}_1} \triangleq E\{\bar{\boldsymbol{z}}_1(n)\bar{\boldsymbol{z}}_1^H(n)\} = \boldsymbol{A}_1(\theta)\boldsymbol{R}_s\boldsymbol{A}_1^H(\theta) + \sigma^2\boldsymbol{I}_p$.

PROOF See Appendix B.

Obviously the expression of $\mathrm{MSE}(\hat{\phi}_k)$ in (50) is more complicated than that of $\mathrm{MSE}(\hat{\theta}_k)$ in (49) due to the fact that the estimated elevation angle $\hat{\theta}_k$ is used to estimate the

azimuth angle ϕ_k and accomplish the pair-matching. As clarified in Appendix B, the first and third terms of MSE($\hat{\phi}_k$) are affected by not only the noise variance σ^2 and the number of snapshots N, but also the estimation error of $\hat{\theta}_k$.

VI. NUMERICAL EXAMPLES

Each ULA of the L-shaped array has $M = 7$ sensors with half-wavelength spacing (i.e., $d = \lambda/2$), and the SNR is defined as the ratio of the signal power to the noise variance at each sensor. For comparing the estimation performance of the CODEC method implemented in the batch manner, some subspace-based 2-D DOA estimation methods developed for the L-shaped array such as the joint SVD-based method (JSVD) [32], the generalized ESPRIT-based joint direction finding (GESPRIT-JDF) [34] and the parallel factor (PARAFAC) analysis model based method (PARAFACM) [35] with automatic pairing, the modified propagation method (MPM) [31] with correct paring, and the cross-correlation matrix based ESPRIT (CCM-ESPRIT) method [37] and the CODE method [40] with pairing-matching are carried out as well, where the PARAFAC decomposition is implemented with the COMFAC Matlab function (cf. [35] and the reference [9] therein). Additionally the 2-D rank reduction estimator (2DRARE) for uniform rectangular array [15] is also applied to the L-shaped array for performance comparison. Note that the computationally intensive eigendecomposition is required in these methods except for the CODE method. All the results shown below are obtained from 20,000 independent trials.

EXAMPLE 1 *Performance versus SNR:* Firstly the constant elevation and azimuth angles of two uncorrelated signals are $(\theta_1, \phi_1) = (50^\circ, 43^\circ)$ and $(\theta_2, \phi_2) = (75^\circ, 53^\circ)$, and the SNRs are varied from –10 dB to 25 dB, while the number of snapshots is fixed at $N = 100$.

The scatter plots of 2-D DOA estimation results for 200 estimates of the 20,000 independent trials at SNR = –2.5 dB are shown in Fig. 3. We can see that the estimate $(\hat{\theta}_k, \hat{\phi}_k)$ deviates from its true location due to the influence of additive noises and the finite number of snapshots, and hence the pair $(\hat{\theta}_k, \hat{\phi}_k)$ lying outside the boundaries of the permissible region depicted in Fig. 2(a) will result in the estimation failure [10]. Obviously the estimation failure is encountered for the MPM [31], JSVD [32], GESPRIT-JDF [34], CCM-ESPRIT [37], 2DRARE [15], PARAFACM [35], and CODE [40], while the estimates of the proposed CODEC method are all inside the permissible region, since the constraint is imposed to alleviate the estimation failure. Additionally we can find that the estimated angles of the CODEC method are much less perturbed from their true locations than that of other methods except for the 2DRARE method, because the eigendecomposition is used in the latter, and the estimates of the MPM and GESPRIT-JDF methods fluctuate wildly.

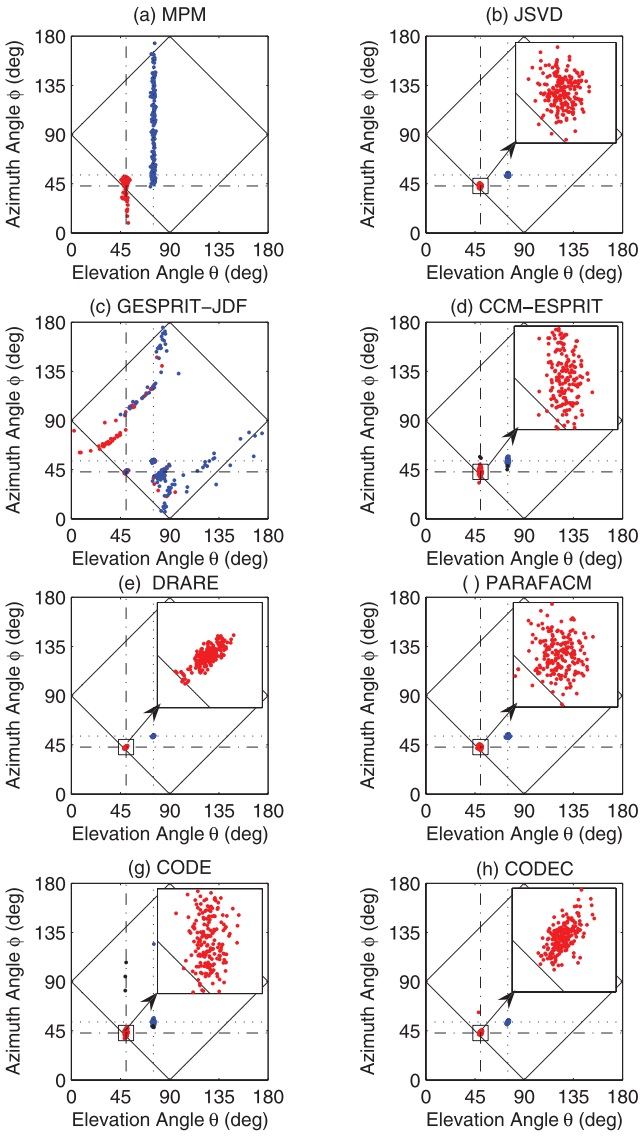

Fig. 3. Scatter plot of two hundred independent estimates for 2-D DOA estimation of two uncorrelated signals (red dot: correct pairing $(\hat{\theta}_1, \hat{\phi}_1)$; blue dot: correct pairing $(\hat{\theta}_2, \hat{\phi}_2)$; black dot: wrong pairing $(\hat{\theta}_1, \hat{\phi}_2)$ or $(\hat{\theta}_2, \hat{\phi}_1)$) in example 1 (SNR = –2.5 dB, $N = 100$, $M = 7$, $(\theta_1, \phi_1) = (50^\circ, 43^\circ)$, and $(\theta_2, \phi_2) = (75^\circ, 53^\circ)$).

Now the empirical root-MSE (RMSE) of the estimated elevation and azimuth angles of the kth signal $s_k(n)$ is employed as the metric of overall performance, which is defined by

$$\text{RMSE} \triangleq \sqrt{\frac{1}{\bar{N}} \sum_{i=1}^{\bar{N}} \left(\left(\theta_k - \hat{\theta}_k^{(i)} \right)^2 + \left(\phi_k - \hat{\phi}_k^{(i)} \right)^2 \right)} \quad (51)$$

where $\bar{N}$ is the number of independent trials (i.e., $\bar{N} =$ 20,000 herein). The empirical RMSEs of $s_2(n)$ are shown in Fig. 4(b), where the theoretical RMSEs of the CODEC method given in (49) and (50) and that of the CODE method [40] and the stochastic Cramer-Rao bound (CRB) [54] are also plotted for comparison, while the detection probabilities of successful pair-matching of the CODE

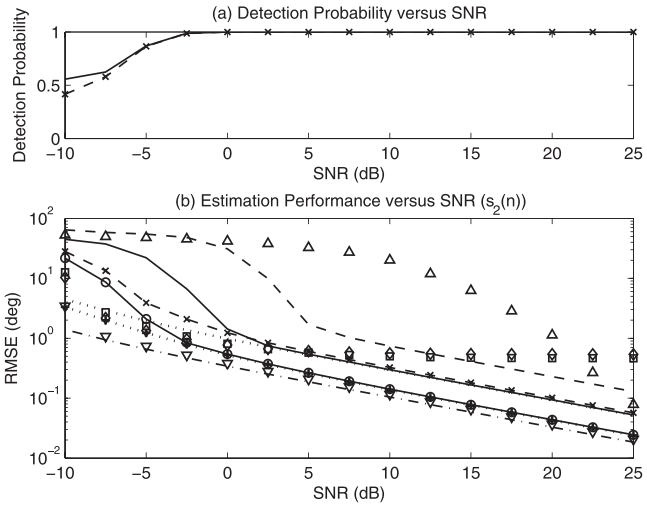

Fig. 4. (a) Detection probability and (b) RMSE of $s_2(n)$ versus SNR for two uncorrelated signals ("◊": JSVD; "Δ": GESPRIT-JDF; "□": PARAFACM; "∇": 2DRARE; dashed line: MPM with correct pairing; dashed line with "x": CCM-ESPRIT; solid line: CODE; solid line with "○": proposed CODEC method; dotted line: theoretical RMSE of CODE; dotted line with "+": theoretical RMSE of CODEC; and dash-dotted line: CRB) in example 1 ($N = 100$, $M = 7$, $(\theta_1, \phi_1) = (50^\circ, 43^\circ)$, and $(\theta_2, \phi_2) = (75^\circ, 53^\circ)$).

method and the CCM-ESPRIT [37] are shown in Fig. 4(a). As clarified in [40], the estimate of the linear propagator in [31, Eq. (17) or (18)] is an approximate solution even when $N \to \infty$, and hence the MPM [31] with correct pairing has larger RMSE regardless of SNR. Although the JSVD [32] performs better at low SNR because of the use of the eigendecomposition process, it has a larger RMSE at moderate to high SNRs due to the inaccurate estimate $\hat{\phi}_k$ caused by the finite number of snapshots (cf. [40]). By introducing two electric angles as the functions of θ_k and ϕ_k, the GESPRIT-JDF [34] employs the generalized ESPRIT method [56] to estimate a "novel electric angle" as a function of these electric angles based on the assumption rank $(\boldsymbol{C}^H\boldsymbol{D}) = \text{rank}(\boldsymbol{D})$. Unfortunately, this relation does not hold true for arbitrary matrices $\boldsymbol{C}$ and $\boldsymbol{D}$ due to the fact that $\text{rank}(\boldsymbol{C}^H\boldsymbol{D}) \leq \min\{\text{rank}(\boldsymbol{C}), \text{rank}(\boldsymbol{D})\}$. Consequently the GESPRIT-JDF has large RMSEs regardless of the SNR and the number of snapshots, even though it invokes two computationally intensive and time-consuming eigendecomposition processes. The PARAFACM [35] is a combination of the PARAFAC [57] with the L-shaped array and developed under the basic assumption that the signal covariance matrix $\boldsymbol{R}_s$ is a diagonal matrix. Clearly the estimated matrix $\boldsymbol{R}_s$ becomes a nondiagonal matrix when the number of snapshots is finite, and hence the PARAFACM provides inaccurate direction estimates even at high SNR and for uncorrelated signals. Further since it involves a multiparameter nonlinear optimization problem, the PARAFACM is rather computationally complicated and requires good initial estimates. We note that the 2DRARE [15] provides more accurate estimates than the other methods because the $2M \times 2M$ covariance matrix of two ULAs (i.e., all correlations) and its eigendecomposition are invoked, while its computational complexity is roughly $32M^2\,N + O(8M^3) + p^2\,(2(M-1)^2 + 6M^2) + 32p^2(M-1)^2 + 2p(M-1)O(p^3) + O(4p^2(M-1)^2) + p(8M + 25M^2 + O((2M + 1)^2))$ flops, which is much larger than that of the proposed CODEC method. Additionally when the SNR is low, some pair-matchings of estimated elevation and azimuth angles fail as shown in Fig. 4(a), and these unsuccessful pair-matchings cause the CCM-ESPRIT [37] and the CODE [40] to degrade at low SNR, while the latter has smaller empirical RMSE than the former at moderate to high SNRs.

However, the proposed CODEC method estimates the elevation angles $\{\theta_k\}$ by using the cross-correlations between two ULAs with the working array aperture M. Then these estimates $\{\hat{\theta}_k\}$ are employed to estimate the corresponding azimuth angles $\{\phi_k\}$ by using some cross-correlations between two ULAs and that between two subarrays with the working array aperture $2M - p$ and by taking the permissible region of parameters θ_k and ϕ_k given in (3). As a result, the CODEC method without eigendecomposition can pair the estimated elevation and azimuth angles automatically, and its estimation performance is better than that of the CODE [40] and the other aforementioned methods [31, 32, 34, 35, 37] except for the 2DRARE with eigendecomposition [15] as displayed in Fig. 4. The relative efficiency ratios between the computational complexity of the CODE/2DRARE and that of the CODEC in MATLAB flops are about $f_{\text{CODE}}/f_{\text{CODEC}} \approx 4.754$ and $f_{\text{2DRARE}}/f_{\text{CODEC}} \approx 7.609$ in this empirical scenario. Further the empirical RMSE of $s_2(n)$ is very close to the theoretical one given in (49) and (50), which is smaller to that of the CODE method, and the difference between the theoretical RMSE and the CRB is small. (The results for $s_1(n)$ are similar and omitted herein).

EXAMPLE 2 *Performance versus Number of Snapshots:* The simulation conditions are similar to those in example 1, except that the number of snapshots N is varied from 10 to 1,000, and the SNR is fixed at SNR = 5 dB. As shown in Fig. 5, it is clear that the proposed CODEC method generally outperforms the MPM [31] with correct pairing, the JSVD [32], GESPRIT-JDF [34], and PARAFACM [35] with automatic pairing, and the CCM-ESPRIT [37] and the CODE method [40] with pair-matching even when the number of snapshots is rather small, while the 2DRARE [15] has relatively better performance than the other methods at low SNR due to the use of eigendecomposition. Furthermore the empirical RMSE agrees very well with the theoretical one derived in Section V (except for a small number of snapshots).

EXAMPLE 3 *Tracking Performance of On-Line Algorithm:* Now there are four uncorrelated signals with the nonlinearly or linearly time-varying elevation and azimuth angles $(\theta_1(n),\phi_1(n))$, $(\theta_2(n),\phi_2(n))$, $(\theta_3(n),\phi_3(n))$, and $(\theta_4(n),\phi_4(n))$ with SNR = 5 dB, where $(\theta_1(0),\phi_1(0)) = (72^\circ, 120^\circ)$, $(\theta_2(0),\phi_2(0)) = (135^\circ, 60^\circ)$, $(\theta_3(0),\phi_3(0))$

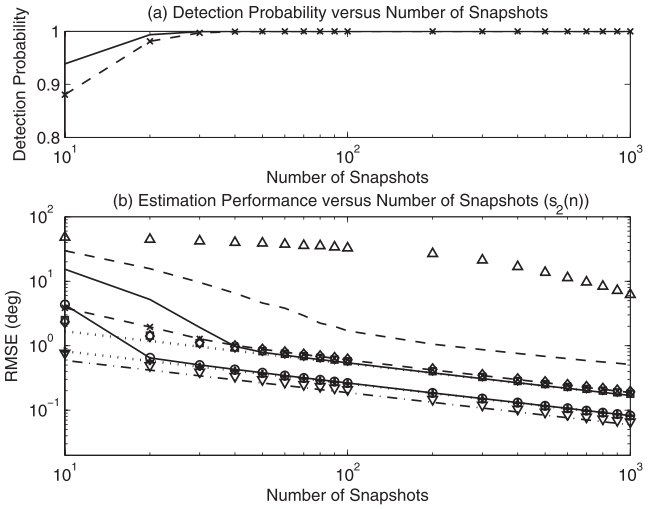

Fig. 5. (a) Detection probability and (b) RMSE of $s_2(n)$ versus number of snapshots for two uncorrelated signals ("◊": JSVD; "Δ": GESPRIT-JDF; "□": PARAFACM; "∇": 2DRARE; dashed line: MPM with correct pairing; dashed line with "x": CCM-ESPRIT; solid line: CODE; solid line with "○": proposed CODEC method; dotted line: theoretical RMSE of CODE; dotted line with "+": theoretical RMSE of CODEC; and dash-dotted line: CRB) in example 2 (SNR = 5 dB, $M = 7$, $(\theta_1, \phi_1) = (50^\circ, 43^\circ)$, and $(\theta_2, \phi_2) = (75^\circ, 53^\circ)$).

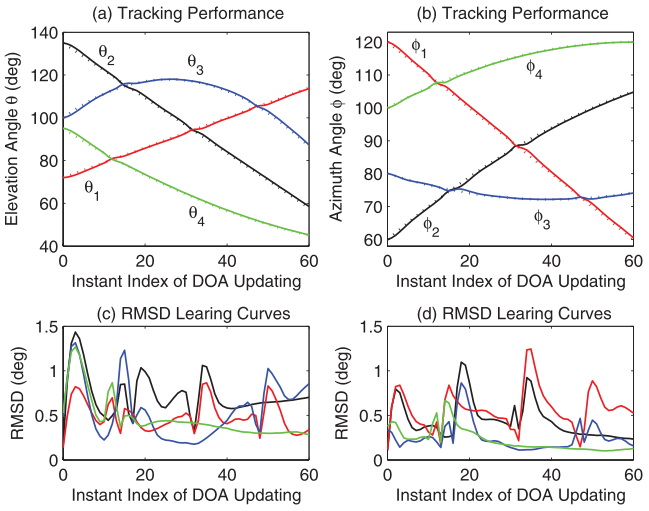

Fig. 6. Averaged estimates of (a) $\theta_k(\bar{n})$ and (b) $\phi_k(\bar{n})$ of four uncorrelated signals with crossings and RMSD learning curves of (c) RMSD($\hat{\theta}_k(\bar{n})$) and RMSD($\hat{\phi}_k(\bar{n})$) in example 3 (dotted line: actual values; red solid lines: $\hat{\theta}_1(\bar{n})$ or $\hat{\phi}_1(\bar{n})$; back solid lines: $\hat{\theta}_2(\bar{n})$ or $\hat{\phi}_2(\bar{n})$; blue solid lines: $\hat{\theta}_3(\bar{n})$ or $\hat{\phi}_3(\bar{n})$; and green solid lines: $\hat{\theta}_4(\bar{n})$ or $\hat{\phi}_4(\bar{n})$; SNR = 5 dB, $M = 7$, $N_s = 200$, and $\bar{\gamma} = 0.99$).

$= (100^\circ, 80^\circ)$, and $(\theta_4(0), \phi_4(0)) = (95^\circ, 100^\circ)$ as shown in Figs. 6(a) and 6(b), and $N_s = 200$. The forgetting factor $\bar{\gamma}$ in (37) and (38) is set as $\bar{\gamma} = 0.99$, and the Luenberger observer gains $\{\boldsymbol{g}_{\theta_k}\}$ and $\{\boldsymbol{g}_{\phi_k}\}$ in (31) and (34) are chosen as $\boldsymbol{g}_{\theta_1} = \boldsymbol{g}_{\phi_1} = [0.5070, 0.1493/N_s, 0.0165/N_s^2]^T$, $\boldsymbol{g}_{\theta_2} = \boldsymbol{g}_{\phi_2} = [0.5070, 0.1399/N_s, 0.0143/N_s^2]^T$, $\boldsymbol{g}_{\theta_3} = \boldsymbol{g}_{\phi_3} = [0.4880, 0.1421/N_s, 0.0156/N_s^2]^T$, and $\boldsymbol{g}_{\theta_4} = \boldsymbol{g}_{\phi_4} = [0.4975, 0.1443/N_s, 0.0157/N_s^2]^T$.

Here we define the empirical root-mean-square derivation (RMSD) learning curve of the estimated azimuth and elevation angles $\hat{\theta}_k(\bar{n})$ and $\hat{\phi}_k(\bar{n})$ as

$$\text{RMSD}(\hat{\phi}_k(\bar{n})) \triangleq \sqrt{\frac{1}{\bar{N}}\sum_{i=1}^{\bar{N}}\left(\phi_k(\bar{n}) - \hat{\phi}_k^{(i)}(\bar{n})\right)^2} \tag{52}$$

$$\text{RMSD}(\hat{\theta}_k(\bar{n})) \triangleq \sqrt{\frac{1}{\bar{N}}\sum_{i=1}^{\bar{N}}\left(\theta_k(\bar{n}) - \hat{\theta}_k^{(i)}(\bar{n})\right)^2} \tag{53}$$

where $\hat{\theta}_k^{(i)}(\bar{n})$ and $\hat{\phi}_k^{(i)}(\bar{n})$ are the estimates obtained in the ith trial at the instant $\bar{n}$. The trajectories of the actual elevation angles and their averaged estimates $\{\hat{\theta}_k(\bar{n})\}$, and their empirical RMSD learning curves are plotted in Figs. 6(a) and 6(c), while the corresponding results for the azimuth angles $\{\phi_k(\bar{n})\}$ are shown in Figs. 6(b) and 6(d), respectively. As described above, because the computationally expensive eigendecomposition process and pair-matching procedure are avoided, the proposed CODEC method is feasible for the on-line implementation. Moreover due to the utilization of the Luenberger state observer, the presented on-line algorithm can achieve correct association of estimates $\hat{\theta}_k(\bar{n})$ and $\hat{\phi}_k(\bar{n})$ at two successive instants of direction updating. From the empirical mean and mean-square behaviors shown in Fig. 6, we can see that the proposed on-line algorithm has a remarkable capability for tracking the time-varying 2-D DOAs of multiple targets with crossings on their trajectories, and the estimated elevation and azimuth angles are always very close to the actual values.

VII. CONCLUSIONS

In this paper, a new computationally efficient subspace-based batch method called CODEC and its on-line algorithm with Luenberger observer were proposed for 2-D DOA estimation and tracking of noncoherent narrowband signals of multiple targets impinging on the L-shaped sensor array, where the computationally expensive eigendecomposition process and pair-matching procedure are avoided, and the estimation failure is overcome. The statistical properties of the CODEC method were studied, and the expressions of asymptotic MSEs of the estimated elevation and azimuth angles were clarified explicitly. Furthermore the effectiveness of the CODEC method and the tracking algorithm and the theoretical analysis were verified through numerical examples. The simulation results showed that the CODEC method implemented in the batch manner outperforms the previously proposed CODE method with pair-matching with a small number of snapshots and at low SNR, and the theoretical analysis agrees well with empirical results, while the on-line algorithm can provide remarkable performance for tracking the 2-D DOAs of multiple moving targets with crossover points on their trajectories.

APPENDIX A. COMPUTATION OF OBSERVER GAIN

Here by defining the gain of Luenberger observer as $\boldsymbol{g} \triangleq [g_1, g_2, g_3]^T$ and letting z_1, z_2, and z_3 denote the desired pole locations of the matrix $\boldsymbol{F} - \boldsymbol{g}\boldsymbol{c}^T\boldsymbol{F}$, we can derive its characteristic equation

$$\begin{aligned}\det\{z\boldsymbol{I}_3 - (\boldsymbol{F} - \boldsymbol{g}c^T\boldsymbol{F})\} &= z^3 + (g_1 + g_2N_s + 0.5g_3N_s^2 - 3)z^2 + (-2g_1 \\ &\quad -g_2N_s + 0.5g_3N_s^2 + 3)z + g_1 + 1 = 0 \end{aligned} \tag{54}$$

while the desired observer characteristic equation is given by

$$(z - z_1)(z - z_2)(z - z_3) = z^3 + c_1z^2 + c_2z + c_3 = 0 \tag{55}$$

where $c_1 \triangleq -(z_1 + z_2 + z_3)$, $c_2 \triangleq z_1z_2 + z_1z_3 + z_2z_3$, and $c_3 \triangleq z_1z_2z_3$. Then by comparing the coefficients of equal powers of z in (54) and (55) and after some simple manipulations, we can obtain the elements of gain $\boldsymbol{g}$ as

$$g_1 = c_3 + 1 \tag{56}$$

$$g_2 = \frac{1}{2N_s}(c_1 - c_2 - 3c_3 + 3) \tag{57}$$

$$g_3 = \frac{1}{N_s^2}(c_1 + c_2 + c_3 + 1). \tag{58}$$

APPENDIX B. PROOF OF THEOREM 1

Firstly we consider the derivation of $\mathrm{MSE}(\hat{\theta}_k)$ in (49). We easily obtain the first-order expression for the estimation error $\Delta\theta_k$ of the estimate $\hat{\theta}_k$ as [40]

$$\begin{aligned}\Delta\theta_k \triangleq \hat{\theta}_k - \theta_k &\approx -\frac{\mathrm{Re}\{\boldsymbol{d}^H(\theta_k)\widehat{\boldsymbol{\Pi}}_z\boldsymbol{a}(\theta_k)\}}{\boldsymbol{d}^H(\theta_k)\boldsymbol{\Pi}_z\boldsymbol{d}(\theta_k)} \\ &\approx -\frac{\mathrm{Re}\{\boldsymbol{d}^H(\theta_k)\boldsymbol{Q}_z(\boldsymbol{Q}_z^H\boldsymbol{Q}_z)^{-1}\widehat{\boldsymbol{Q}}_z^H\boldsymbol{a}(\theta_k)\}}{H_{zkk}} \\ &= -\frac{\mathrm{Re}\{\nu_k\}}{H_{zkk}}\end{aligned} \tag{59}$$

where $\widetilde{\boldsymbol{d}}(\theta) \triangleq d\boldsymbol{d}(\theta)/d\theta$, the estimated orthogonal projector $\widehat{\boldsymbol{\Pi}}_z$ in the denominator of (59) can be replaced with the true $\boldsymbol{\Pi}_z$ without affecting the asymptotic property of estimate $\hat{\theta}_k$ (cf. [39, 46, 47]), and

$$\begin{aligned}\nu_k &\triangleq \boldsymbol{d}^H(\theta_k)\boldsymbol{Q}_z(\boldsymbol{Q}_z^H\boldsymbol{Q}_z)^{-1}\widehat{\boldsymbol{Q}}_z^H\boldsymbol{a}(\theta_k) \\ &\approx -\boldsymbol{d}^H(\theta_k)\boldsymbol{\Pi}_z\widehat{\boldsymbol{R}}_z\boldsymbol{R}_{z1}^H(\boldsymbol{R}_{z1}\boldsymbol{R}_{z1}^H)^{-1}\boldsymbol{a}_1(\theta_k) \\ &= -\boldsymbol{g}^H(\theta_k)[\widehat{\boldsymbol{R}}_{zx}, \widehat{\widetilde{\boldsymbol{R}}}_{zx}][\boldsymbol{R}_{\bar{z}_1x}, \widetilde{\boldsymbol{R}}_{\bar{z}_1x}]^H(\boldsymbol{R}_{z1}\boldsymbol{R}_{z1}^H)^{-1}\boldsymbol{a}_1(\theta_k) \\ &= \nu_{k1} + \nu_{k2}\end{aligned} \tag{60}$$

in which

$$\nu_{k1} \triangleq -\frac{1}{N}\sum_{n=1}^{N}\boldsymbol{g}^H(\theta_k)\boldsymbol{z}(n)\boldsymbol{x}^H(n)\boldsymbol{h}(\theta_k) \tag{61}$$

$$\begin{aligned}\nu_{k2} &\triangleq -\boldsymbol{g}^H(\theta_k)\widehat{\widetilde{\boldsymbol{R}}}_{zx}\overline{\boldsymbol{h}}(\theta_k) \\ &= -\frac{1}{N}\sum_{n=1}^{N}\boldsymbol{g}^H(\theta_k)\boldsymbol{J}_M\boldsymbol{z}^*(n)\boldsymbol{x}^T(n)\overline{\boldsymbol{h}}(\theta_k).\end{aligned} \tag{62}$$

Consequently from (59), the MSE of the estimation error $\Delta\theta_k$ is given by

$$\mathrm{MSE}(\theta_k) \triangleq E\{(\Delta\theta_k)^2\} \approx \frac{1}{2H_{zkk}^2}\mathrm{Re}\{E\{\nu_k^2\} + E\{|\nu_k|^2\}\} \tag{63}$$

where the fact that $\mathrm{Re}\{\nu_i\}\mathrm{Re}\{\nu_k\} = 0.5(\mathrm{Re}\{\nu_i\nu_k\} + \mathrm{Re}\{\nu_i\nu_k^*\})$ is used implicitly. Thus by substituting (60) into (63) and performing some lengthy but straightforward manipulations under the assumptions of data model, $\mathrm{MSE}(\theta_k)$ in (49) can be readily obtained (see [40] for details).

On the other hand, as the azimuth angle $\hat{\phi}_k$ is a minimum point of $f_k(\phi)$ in (20), by considering the relationship between the cost functions $f_k(\phi)$ in (20) and $f(\theta, \phi)$ in (19), we get

$$0 = f_k'(\hat{\phi}_k) = f_\phi'(\hat{\theta}_k, \hat{\phi}_k) \tag{64}$$

where $f_\phi'(\theta, \phi)$ is the first-order partial derivative of $f(\theta, \phi)$ in (19) with respect to ϕ given by

$$f_\phi'(\theta, \phi) \triangleq \frac{\partial f(\theta, \phi)}{\partial\phi} = 2\mathrm{Re}\{\overline{\boldsymbol{d}}_\phi^H(\theta, \phi)\widehat{\overline{\boldsymbol{\Pi}}}\overline{\boldsymbol{a}}^H(\theta, \phi)\}\} \tag{65}$$

in which $\overline{\boldsymbol{d}}_\phi(\theta, \phi) = [\boldsymbol{0}_{(M-p)\times 1}^T, \boldsymbol{d}^T(\phi)]^T$. Since $\hat{\theta}_k$ and $\hat{\phi}_k$ are consistent estimates for a sufficiently large number of snapshots N, the approximation of $f_\phi'(\hat{\theta}_k, \hat{\phi}_k)$ can be found in its Taylors series expansion about the true values θ_k and ϕ_k as

$$\begin{aligned}f_\phi'(\hat{\theta}_k, \hat{\phi}_k) \approx\ & f_\phi'(\theta_k, \phi_k) + f_{\phi\phi}''(\theta_k, \phi_k)(\hat{\phi}_k - \phi_k) \\ & + f_{\phi\theta}''(\theta_k, \phi_k)(\hat{\theta} - \theta_k)\end{aligned} \tag{66}$$

where the second-order partial derivatives $f_{\phi\theta}''(\theta, \phi)$ and $f_{\phi\phi}''(\theta, \phi)$ of $f(\theta, \phi)$ are given by

$$\begin{aligned}f_{\phi\theta}''(\theta, \phi) &\triangleq \frac{\partial f_\phi'(\theta, \phi)}{\partial\theta} \\ &= 2\mathrm{Re}\{\widetilde{\boldsymbol{d}}_{\phi\theta}^H(\theta, \phi)\widehat{\overline{\boldsymbol{\Pi}}}\overline{\boldsymbol{a}}(\theta, \phi) \\ &\quad + \overline{\boldsymbol{d}}_\phi^H(\theta, \phi)\widehat{\overline{\boldsymbol{\Pi}}}\overline{\boldsymbol{d}}_\theta(\theta, \phi)\} \\ &= 2\mathrm{Re}\{\overline{\boldsymbol{d}}_\phi^H(\theta, \phi)\widehat{\overline{\boldsymbol{\Pi}}}\overline{\boldsymbol{d}}_\theta(\theta, \phi)\}\end{aligned} \tag{67}$$

$$\begin{aligned}f_{\phi\phi}''(\theta, \phi) &\triangleq \frac{\partial f_\phi'(\theta, \phi)}{\partial\phi} \\ &= 2\mathrm{Re}\{\widetilde{\boldsymbol{d}}_{\phi\phi}^H(\theta, \phi)\widehat{\overline{\boldsymbol{\Pi}}}\overline{\boldsymbol{a}}(\theta, \phi) \\ &\quad + \overline{\boldsymbol{d}}_\phi^H(\theta, \phi)\widehat{\overline{\boldsymbol{\Pi}}}\overline{\boldsymbol{d}}_\phi(\theta, \phi)\} \\ &\approx 2\mathrm{Re}\{\overline{\boldsymbol{d}}_\phi^H(\theta, \phi)\widehat{\overline{\boldsymbol{\Pi}}}\overline{\boldsymbol{d}}_\phi(\theta, \phi)\}\end{aligned} \tag{68}$$

in which $\overline{\boldsymbol{d}}_\theta(\theta, \phi) = [\boldsymbol{d}_2^T(\theta), \boldsymbol{0}_{M\times 1}^T]^T$, and $\widetilde{\boldsymbol{d}}_{\phi\theta} = 0$ is used implicitly in (67). From (66) and (59), we can obtain the

estimate error $\Delta\phi \triangleq \hat{\phi}_k - \phi_k$ as

$$\begin{aligned}\Delta\phi_k &\triangleq \hat{\phi}_k - \phi_k \\ &\approx -\frac{1}{f''_{\phi\phi}(\theta_k,\phi_k)}\left(f'_{\phi}(\theta_k,\phi_k) - f''_{\phi\theta}(\theta_k,\phi_k)\frac{\mathrm{Re}\{\nu_k\}}{H_{zkk}}\right) \\ &\approx -\frac{1}{\overline{\boldsymbol{d}}^H_{\phi}(\theta_k,\phi_k)\overline{\boldsymbol{\Pi}}\overline{\boldsymbol{d}}_{\phi}(\theta_k,\phi_k)} \\ &\quad\cdot(\mathrm{Re}\{\overline{\boldsymbol{d}}^H_{\phi}(\theta_k,\phi_k)\widehat{\overline{\boldsymbol{\Pi}}}\bar{\boldsymbol{a}}^H(\theta_k,\phi_k)\} \\ &\quad -\mathrm{Re}\{\overline{\boldsymbol{d}}^H_{\phi}(\theta_k,\phi_k)\overline{\boldsymbol{\Pi}}\overline{\boldsymbol{d}}_{\theta}(\theta_k,\phi_k)\}\frac{\mathrm{Re}\{\nu_k\}}{H_{zkk}}) \\ &= -\frac{1}{\tilde{H}_{kk}}\left(\mathrm{Re}\{\xi_k\} + \bar{H}_{kk}\frac{\mathrm{Re}\{\nu_k\}}{H_{zkk}}\right) \end{aligned} \tag{69}$$

where the estimated orthogonal projector $\widehat{\overline{\boldsymbol{\Pi}}}$ in the second-order derivatives $f''_{\phi\phi}(\theta_k,\phi_k)$ and $f''_{\phi\theta}(\theta_k,\phi_k)$ are replaced with the true $\overline{\boldsymbol{\Pi}}$ without affecting the asymptotic property of estimate $\hat{\phi}_k$ similarly to that used in (59), while

$$\begin{aligned}\tilde{H}_{kk} &\triangleq \overline{\boldsymbol{d}}^H_{\phi}(\theta_k,\phi_k)\overline{\boldsymbol{\Pi}}\overline{\boldsymbol{d}}_{\phi}(\theta_k,\phi_k) \\ &= \boldsymbol{d}^H(\phi_k)\overline{\boldsymbol{\Pi}}_{22}\boldsymbol{d}(\phi_k)\end{aligned} \tag{70}$$

$$\begin{aligned}\bar{H}_{kk} &\triangleq -\mathrm{Re}\{\overline{\boldsymbol{d}}^H_{\phi}(\theta_k,\phi_k)\overline{\boldsymbol{\Pi}}\overline{\boldsymbol{d}}_{\theta}(\theta_k,\phi_k)\} \\ &= -\mathrm{Re}\{\boldsymbol{d}^H(\phi_k)\overline{\boldsymbol{\Pi}}_{21}\boldsymbol{d}_2(\theta_k)\} \\ &= \mathrm{Re}\{\boldsymbol{d}^H(\phi_k)\boldsymbol{A}(\phi)(\overline{\boldsymbol{A}}^H(\theta,\phi)\overline{\boldsymbol{A}}(\theta,\phi))^{-1}A_2^H(\theta)\boldsymbol{d}_2(\theta_k)\}\end{aligned} \tag{71}$$

$$\xi_k \triangleq \overline{\boldsymbol{d}}^H_{\phi}(\theta_k,\phi_k)\widehat{\overline{\boldsymbol{\Pi}}}\bar{\boldsymbol{a}}^H(\theta_k,\phi_k) \tag{72}$$

in which remark 3 and (24) are used implicitly.

Furthermore the estimated orthogonal projector $\widehat{\overline{\boldsymbol{\Pi}}}$ in (72) can be approximated as (cf. [39, 47])

$$\begin{aligned}\widehat{\overline{\boldsymbol{\Pi}}} &= \boldsymbol{I}_{2M-p} - \widehat{\overline{\boldsymbol{R}}}(\widehat{\overline{\boldsymbol{R}}}^H\widehat{\overline{\boldsymbol{R}}})^{-1}\widehat{\overline{\boldsymbol{R}}}^H \\ &\approx \boldsymbol{I}_{2M-p} - (\widehat{\overline{\boldsymbol{R}}} - \overline{\boldsymbol{R}})(\overline{\boldsymbol{R}}^H\overline{\boldsymbol{R}})^{-1}\overline{\boldsymbol{R}}^H - \overline{\boldsymbol{R}}(\widehat{\overline{\boldsymbol{R}}}^H\widehat{\overline{\boldsymbol{R}}})^{-1}\widehat{\overline{\boldsymbol{R}}}^H\end{aligned} \tag{73}$$

where

$$\overline{\boldsymbol{R}}(\widehat{\overline{\boldsymbol{R}}}^H\widehat{\overline{\boldsymbol{R}}})^{-1}\widehat{\overline{\boldsymbol{R}}}^H \approx \overline{\boldsymbol{R}}(\overline{\boldsymbol{R}}^H\overline{\boldsymbol{R}})^{-1}(\widehat{\overline{\boldsymbol{R}}} - \overline{\boldsymbol{R}})^H + \overline{\boldsymbol{R}}(\widehat{\boldsymbol{R}}^H\widehat{\overline{\boldsymbol{R}}})^{-1}\overline{\boldsymbol{R}}^H \tag{74}$$

in which

$$\begin{aligned}\overline{\boldsymbol{R}}(\widehat{\overline{\boldsymbol{R}}}^H\widehat{\overline{\boldsymbol{R}}})^{-1}\overline{\boldsymbol{R}}^H &\approx \overline{\boldsymbol{R}}(\overline{\boldsymbol{R}}^H\overline{\boldsymbol{R}})^{-1}(\overline{\boldsymbol{R}}^H\overline{\boldsymbol{R}} - \widehat{\overline{\boldsymbol{R}}}^H\widehat{\overline{\boldsymbol{R}}})(\overline{\boldsymbol{R}}^H\overline{\boldsymbol{R}})^{-1}\overline{\boldsymbol{R}}^H \\ &\quad + (\boldsymbol{I}_{2M-p} - \overline{\boldsymbol{\Pi}})\end{aligned} \tag{75}$$

and

$$\overline{\boldsymbol{R}}^H\overline{\boldsymbol{R}} - \widehat{\overline{\boldsymbol{R}}}^H\widehat{\overline{\boldsymbol{R}}} \approx 2\overline{\boldsymbol{R}}^H\overline{\boldsymbol{R}} - \overline{\boldsymbol{R}}^H\widehat{\overline{\boldsymbol{R}}} - \widehat{\overline{\boldsymbol{R}}}^H\overline{\boldsymbol{R}}. \tag{76}$$

By combining (73)–(76) and after some simple calculations, we get the approximation of $\widehat{\overline{\boldsymbol{\Pi}}}$ as

$$\widehat{\overline{\boldsymbol{\Pi}}} \approx (\boldsymbol{I}_{2M-P} - \overline{\boldsymbol{R}}(\overline{\boldsymbol{R}}^H\overline{\boldsymbol{R}})^{-1}\widehat{\overline{\boldsymbol{R}}}^H)\overline{\boldsymbol{\Pi}} - \overline{\boldsymbol{\Pi}}\widehat{\overline{\boldsymbol{R}}}(\overline{\boldsymbol{R}}^H\overline{\boldsymbol{R}})^{-1}\overline{\boldsymbol{R}}^H. \tag{77}$$

Then by substituting (77) into (72) and using the fact $\overline{\boldsymbol{\Pi}}\bar{\boldsymbol{a}}(\theta_k,\phi_k) = \boldsymbol{0}_{(2M-p)\times 1}$, from (16), ξ_k can be approximated as

$$\begin{aligned}\xi_k &\approx -\overline{\boldsymbol{d}}^H_{\phi}(\theta_k,\phi_k)\widehat{\overline{\boldsymbol{\Pi}}}\widehat{\overline{\boldsymbol{R}}}(\overline{\boldsymbol{R}}^H\overline{\boldsymbol{R}})^{-1}\overline{\boldsymbol{R}}^H\bar{\boldsymbol{a}}(\theta_k,\phi_k) \\ &= -\bar{\boldsymbol{g}}^H(\theta_k,\phi_k)\widehat{\overline{\boldsymbol{R}}}\boldsymbol{b}(\theta_k,\phi_k) \\ &= -\frac{1}{N}\sum_{n=1}^{N}\bar{\boldsymbol{g}}^H(\theta_k,\phi_k)\bar{\boldsymbol{y}}(n)\bar{\boldsymbol{z}}_1^H(n)\boldsymbol{b}(\theta_k,\phi_k)\end{aligned} \tag{78}$$

where

$$\bar{\boldsymbol{g}}(\theta_k,\phi_k) \triangleq \overline{\boldsymbol{\Pi}}\overline{\boldsymbol{d}}_{\phi}(\theta_k,\phi_k) = [\overline{\boldsymbol{\Pi}}_{12}^T, \overline{\boldsymbol{\Pi}}_{22}^T]^T\boldsymbol{d}(\phi_k) \tag{79}$$

$$\begin{aligned}\boldsymbol{b}(\theta_k,\phi_k) &\triangleq (\overline{\boldsymbol{R}}^H\overline{\boldsymbol{R}})^{-1}\overline{\boldsymbol{R}}^H\bar{\boldsymbol{a}}(\theta_k,\phi_k) \\ &= (\boldsymbol{R}_s\boldsymbol{A}_1(\theta)^H)^{-1}(\overline{\boldsymbol{A}}^H(\theta,\phi)\overline{\boldsymbol{A}}(\theta,\phi))^{-1} \\ &\quad\times\overline{\boldsymbol{A}}^H(\theta,\phi)\bar{\boldsymbol{a}}(\theta_k,\phi_k) \\ &= (\boldsymbol{R}_s\boldsymbol{A}_1^H(\theta))^{-1}\boldsymbol{e}_k.\end{aligned} \tag{80}$$

Consequently from (69) and (63), the MSE of the estimation error $\Delta\phi_k$ is given by

$$\begin{aligned}\mathrm{MSE}(\hat{\phi}_k) &\triangleq E\{(\Delta\phi_k)^2\} \\ &= \frac{\tilde{H}_{kk}^2}{\tilde{H}_{kk}^2}\mathrm{MSE}(\hat{\theta}_k) + \frac{1}{2\tilde{H}_{kk}^2}\mathrm{Re}\{E\{\xi_k^2\} + E\{|\xi_k|^2\}\} \\ &\quad + \frac{\bar{H}_{kk}}{\tilde{H}_{kk}^2 H_{zkk}}\mathrm{Re}\{E\{\xi_k\nu_k\} + E\{\xi_k\nu_k^*\}\}.\end{aligned} \tag{81}$$

Under the basic assumptions on the data model, and by using the well-known formula for the expectation of four Gaussian random variables with zero-mean (e.g., [55])

$$\begin{aligned}E\{x_1x_2x_3x_4\} &= E\{x_1x_2\}E\{x_3x_4\} \\ &\quad + E\{x_1x_3\}E\{x_2x_4\} + E\{x_1x_4\}E\{x_2x_3\}\end{aligned}$$

and considering the facts that $\overline{\boldsymbol{\Pi}}\bar{\boldsymbol{a}}(\theta_k,\phi_k) = \boldsymbol{0}_{(2M-p)\times 1}$ and $\boldsymbol{\Pi}_z\bar{\boldsymbol{a}}(\theta_k) = \boldsymbol{0}_{M\times 1}$, from (60) and (78), we can get

$$\begin{aligned}E\{\xi_k^2\} &= \frac{1}{N^2}E\left\{\sum_{n=1}^{N}\sum_{t=1}^{N}\bar{\boldsymbol{g}}^H(\theta_k,\phi_k)\bar{\boldsymbol{y}}(n)\bar{\boldsymbol{z}}_1^H(n)\boldsymbol{b}(\theta_k,\phi_k)\right. \\ &\quad\left.\times\bar{\boldsymbol{g}}^H(\theta_k,\phi_k)\bar{\boldsymbol{y}}(t)\bar{\boldsymbol{z}}_1^H(t)\boldsymbol{b}(\theta_k,\phi_k)\right\} \\ &= \bar{\boldsymbol{g}}^H(\theta_k,\phi_k)\overline{\boldsymbol{R}}\boldsymbol{b}(\theta_k,\phi_k)\bar{\boldsymbol{g}}^H(\theta_k,\phi_k)\overline{\boldsymbol{R}}\boldsymbol{b}(\theta_k,\phi_k) \\ &\quad + 0 + \frac{1}{N}\bar{\boldsymbol{g}}^H(\theta_k,\phi_k)\overline{\boldsymbol{R}}\boldsymbol{b}(\theta_k,\phi_k)\bar{\boldsymbol{g}}^H(\theta_k,\phi_k) \\ &\quad\times\overline{\boldsymbol{R}}\boldsymbol{b}(\theta_k,\phi_k) = 0.\end{aligned} \tag{82}$$

Similarly we also obtain

$$E\{|\xi_k|^2\} = \frac{\sigma^2}{N}\tilde{H}_{kk}\boldsymbol{b}^H(\theta_k,\phi_k)\boldsymbol{R}_{\bar{z}_1\bar{z}_1}\boldsymbol{b}(\theta_k,\phi_k) \tag{83}$$

$$E\{\xi_k\nu_{k1}\} = \frac{\sigma^4}{N}\bar{\boldsymbol{g}}^H(\theta_k,\phi_k)\boldsymbol{\Gamma}\boldsymbol{h}(\theta_k)\boldsymbol{g}^H(\theta_k)\overline{\boldsymbol{\Gamma}}\boldsymbol{b}(\theta_k,\phi_k) \tag{84}$$

$$E\{\xi_k\nu_{k1}^*\} = \frac{\sigma^2}{N}\bar{\boldsymbol{g}}^H(\theta_k,\phi_k)\widetilde{\boldsymbol{\Gamma}}\boldsymbol{g}(\theta_k)\boldsymbol{h}^H(\theta_k)\boldsymbol{R}^H_{\bar{z}_1x}\boldsymbol{b}(\theta_k,\phi_k) \tag{85}$$

$$E\{\xi_k v_{k2}\} = \frac{\sigma^2}{N}\bar{\boldsymbol{g}}^H(\theta_k,\phi_k)\widetilde{\boldsymbol{\Gamma}}\boldsymbol{J}_M\boldsymbol{g}^*(\theta_k)\overline{\boldsymbol{h}}^T(\theta_k)\boldsymbol{R}^H_{\bar{z}_1 x}\boldsymbol{b}(\theta_k,\phi_k) \tag{86}$$

$$E\{\xi_k v^*_{k2}\} = \frac{\sigma^4}{N}\bar{\boldsymbol{g}}^H(\theta_k,\phi_k)\boldsymbol{\Gamma}\overline{\boldsymbol{h}}^*(\theta_k)\boldsymbol{g}^T(\theta_k)\boldsymbol{J}_M\overline{\boldsymbol{\Gamma}}\boldsymbol{b}(\theta_k,\phi_k) \tag{87}$$

where $\overline{\boldsymbol{\Pi}}\,\overline{\boldsymbol{\Pi}} = \overline{\boldsymbol{\Pi}}$ and $\bar{\boldsymbol{g}}^H(\theta_k,\phi_k)\overline{\boldsymbol{A}}(\theta_k,\phi_k) = \boldsymbol{0}_{1\times p}$ are used implicitly. Therefore by substituting (82)–(87) into (81), $\mathrm{MSE}(\hat{\phi}_k)$ in (50) can be obtained immediately.

ACKNOWLEDGMENT

The authors would like to thank the associate editor Dr. Tod Luginbuhl for his careful review, thoughtful comments, and valuable suggestions that improved the manuscript.

REFERENCES

[1] Bar-Shalom, Y., and Fortmann, T. E.
Tracking and Data Association. New York: Academic Press, 1988.

[2] Gershman, A. B., Rübsamen, M., and Pesavento, M.
One- and two-dimensional direction-of-arrival estimation: An overview of search-free techniques.
Signal Processing, **90**, 5 (May 2010), 1338–1349.

[3] Clark, M. P., and Scharf, L. L.
Two-dimensional modal analysis based on maximum likelihood.
IEEE Transactions on Signal Processing, **42**, 6 (Jun. 1994), 1443–1452.

[4] Rao, C. R., Zhao, L., and Zhou, B.
Maximum likelihood estimation of 2-D superimposed exponential signals.
IEEE Transactions on Signal Processing, **42**, 7 (Jul. 1994), 1795–1802.

[5] van der Veen, A. J., Ober, P. B., and Deprettere, E. F.
Azimuth and elevation computation in high resolution DOA estimation.
IEEE Transactions on Signal Processing, **40**, 7 (Jul. 1992), 1828–1832.

[6] Swindlehurst, A., and Kailath, T.
Azimuth/elevation direction finding using regular array geometries.
IEEE Transactions on Aerospace and Electronic Systems, **29**, 1 (Jan. 1993), 145–156.

[7] Mathews, C. P., and Zoltowski, M. D.
Eigenstructure techniques for 2-D angle estimation with uniform circular arrays.
IEEE Transactions on Signal Processing, **42**, 9 (Sep. 1994), 2395–2407.

[8] Zoltowski, M. D., Haardt, M., and Mathews, C. P.
Closed-form 2-D angle estimation with rectangular arrays in element space or beamspace via unitary ESPRIT.
IEEE Transactions on Signal Processing, **44**, 2 (Feb. 1996), 316–328.

[9] Chen, Y.-M.
On spatial smooting for two-dimensional direction-of-arrival estimation of coherent signals.
IEEE Transactions on Signal Processing, **45**, 7 (Jul. 1997), 1689–1696.

[10] Liu, T.-H., and Mendel, J. M.
Azimuth and elevation direction finding using arbitrary array geometries.
IEEE Transactions on Signal Processing, **46**, 7 (Jul. 1998), 2061–2065.

[11] Hua, Y.
Estimating two-dimensional frequencies by matrix enhancement and matrix pencil.
IEEE Transactions on Signal Processing, **40**, 9 (Sep. 1992), 2267–2280.

[12] Rouquette, S., and Najim, M.
Estimation of frequencies and damping factors by two-dimensional ESPRIT type methods.
IEEE Transactions on Signal Processing, **49**, 1 (Jan. 2001), 237–245.

[13] Hatke, G. F., and Forsythe, K. W.
A class of polynomial rooting algorithms for joint azimuth/elevation estimation using multidimensional arrays.
Proceedings of IEEE 28th Asilomar Conference on Signals, Systems and Computers, Vol. 1, Pacific Grove, CA, Oct. 1994, pp. 694–699.

[14] Li, J., Stoica, P., and Zheng, D.
An efficient algorithm for two-dimensional frequency estimation.
Multidimensional Systems and Signal Processing, **7**, 2 (Apr. 1996), 151–178.

[15] Pesavento, M., and Böhme, J. F.
Eigenstructure-based azimuth and elevation estimation in sparse uniform rectangular arrays.
Proceedings of IEEE 2nd Sensor Array and Multichannel Signal Processing Workshop, Rosslyn, VA, Aug. 2002, pp. 327–331.

[16] Rao, C. R., Sastry, C. R., and Zhou, B.
Tracking the direction of arrival of multiple moving targets.
IEEE Transactions on Signal Processing, **42**, 5 (May 1994), 1133–1144.

[17] Xin, J., and Sano, A.
Directions-of-arrival tracking of coherent cyclostationary signals in array processing.
IEICE Transactions on Fundamentals of Electronics, Communications and Computer Sciences, **E86-A**, 8 (Aug. 2003), 2037–2046.

[18] Xin, J., and Sano, A.
Efficient subspace-based algorithm for adaptive bearing estimation and tracking.
IEEE Transactions on Signal Processing, **53**, 12 (Dec. 2005), 4485–4505.

[19] Xin, J., Zheng, N., and Sano, A.
Subspace-based adaptive method for estimating direction-of-arrival with Luenberger observer.
IEEE Transactions on Signal Processing, **59**, 1 (Jan. 2011), 145–159.

[20] Lo, K. W.
Tracking multiple targets in 2-D angular space using sensor array.
Electronics Letters, **27**, 16 (Aug. 1991), 1478–1480.

[21] Chen, Y.-H., and Lian, Y.-T.
2-D multitarget angle tracking algorithm using sensor array.
IEE Proceedings - Radar, Sonar and Navigation, **142**, 4 (Aug. 1995), 158–161.

[22] Liu, J., and Liu, X.
Joint 2-D tracking for multiple moving targets using adaptive frequency estimation.
Proceedings of 2007 IEEE International Conference on Acoustics, Speech, and Signal Processing, Vol. II, Honolulu, HI, Apr. 2007, pp. 1113–1116.

[23] Sward, C. K., Simaan, M., and Kamen, E. W.
Multiple target angle tracking using sensor array output.
IEEE Transactions on Aerospace and Electronic Systems, **26**, 2 (Mar. 1990), 367–372.

[24] Sastry, C. R., Kamen, E. W., and Simaan, M.
An efficient algorithm for tracking the angles of arrival of moving targets.
IEEE Transactions on Signal Processing, **39**, 1 (Jan. 1991), 242–246.

[25] Liu, J., and Liu, X.
An eigenvector-based approach for multidimensional frequency estimation with improved identifiability.
IEEE Transactions on Signal Processing, **54**, 12 (Dec. 2006), 4543–4556.

[26] Schmidt, R. O.
Multiple emitter location and signal parameter estimation.
IEEE Transactions on Antennas and Propagation, **AP-34**, 3 (Mar. 1986), 276–280.

[27] Strobach, P.
Low-rank adaptive filters.
IEEE Transactions on Signal Processing, **44**, 12 (Dec. 1996), 2932–2947.

[28] Swindlehurst, A. L., Stoica, P., and Jansson, M.
Exploiting arrays with multiple invariances using MUSIC and MODE.
IEEE Transactions on Signal Processing, **49**, 11 (Nov. 2001), 2511–2521.

[29] Hua, Y., Sarkar, T. K., and Weiner, D. D.
An L-shaped array for estimating 2-D directions of wave arrival.
IEEE Transactions on Antennas and Propagation, **39**, 2 (Feb. 1991), 143–146.

[30] Fernández del Río, J. E., and Cátedra-Pérez, M. F.
The matrix pencil method for two-dimensional direction of arrival estimation employing an L-shaped array.
IEEE Transactions on Antennas and Propagation, **45**, 11 (Nov. 1997), 1693–1697.

[31] Tayem, N., and Kwon, H. M.
L-shape 2-dimensional arrival angle estimation with propagator method.
IEEE Transactions on Antennas and Propagation, **53**, 5 (May 2005), 1622–1630.

[32] Gu, J.-F., and Wei, P.
Joint SVD of two cross-correlation matrices to achieve automatic pairing in 2-D angle estimation problems.
IEEE Antennas and Wireless Propagation Letters, **6** (2007), 553–556.

[33] Al-Jazzar, S. O., McLernon, D. C., and Smadi, M. A.
SVD-based joint azimuth/elevation estimation with automatic pairing.
Signal Processing, **90**, 5 (May 2010), 1669–1675.

[34] Liang, J., and Liu, D.
Joint elevation and azimuth direction finding using L-shaped array.
IEEE Transactions on Antennas and Propagation, **58**, 6 (Jun. 2010), 2136–2141.

[35] Liu, D., and Liang, J.
L-shaped array-based 2-D DOA estimation using parallel factor analysis.
Proceedings of 8th World Congress on Intelligent Control and Automation, Jinan, China, Jul. 2010, pp. 6949–6952.

[36] Hua, Y., and Abed-Meraim, K.
Techniques of eigenvalues estimation and association.
Digital Signal Processing, **7**, 4 (Oct. 1997), 253–259.

[37] Kikuchi, S., Tsuji, H., and Sano, A.
Pair-matching method for estimating 2-D angle of arrival with a cross-correlation matrix.
IEEE Antennas and Wireless Propagation Letters, **5**, 1 (Dec. 2006), 35–40.

[38] Comon, P., and Golub, G. H.
Tracking a few extreme singular values and vectors in signal processing.
Proceedings of the IEEE, **78**, 8 (Aug. 1990), 1327–1343.

[39] Xin, J., and Sano, A.
Computationally efficient subspace-based method for direction-of-arrival estimation without eigendecomposition.
IEEE Transactions on Signal Processing, **52**, 4 (Apr. 2004), 876–893.

[40] Wang, G., Xin, J., Zheng, N., and Sano, A.
Computationally efficient subspace-based method for two-dimensional direction estimation with L-shaped array.
IEEE Transactions on Signal Processing, **59**, 7 (Jul. 2011), 3197–3212.

[41] Luenberger, D. G.
Observing the state of a linear system.
IEEE Transactions on Military Electronics, **8**, 2 (Apr. 1964), 74–80.

[42] Xin, J., Zheng, N., and Sano, A.
Simple and efficient nonparametric method for estimating the number of signals without eigendecomposition.
IEEE Transactions on Signal Processing, **55**, 4 (Apr. 2007), 1405–1420.

[43] Liu, J., Xin, J. Zheng, N., and Sano, A.
Detection of the number of coherent narrowband signals with L-shaped sensor array.
Proceedings of IEEE 10th International Conference on Signal Processing, Beijing, China, Oct. 2010, pp. 323–326.

[44] Roy, R., and Kalaith, T.
ESPRIT—Estimation of signal parameters via rational invariance techniques.
IEEE Transactions on Acoustics, Speech, and Signal Processing, **37**, 7 (Jul. 1989), 984–995.

[45] Marcos, S., Marsal, A., and Benider, M.
The propagator method for sources bearing estimation.
Signal Processing, **42**, 2 (Mar. 1995), 121–138.

[46] Stoica, P., and Sharman, K. C.
Maximum likelihood methods for direction-of-arrival estimation.
IEEE Transactions on Acoustics, Speech, and Signal Processing, **38**, 7 (Jul. 1990), 1132–1143.

[47] Stoica, P., and Söderström, T.
Statistical analysis of a subspace method for bearing estimation without eigendecomposition.
IEE Proceedings F, Radar and Signal Processing, **139**, 4 (Aug. 1992), 301–305.

[48] Rao, B. D., and Hari, K. V. S.
Performance analysis of root-MUSIC.
IEEE Transactions on Acoustics, Speech, and Signal Processing, **37**, 12 (Dec. 1989), 1939–1949.

[49] Orchard, H. J.
The Laguerre method for finding the zeros of polynomials.
IEEE Transactions on Circuits and Systems, **36**, 11 (Nov. 1989), 1377–1381.

[50] Lang, M., and Frenzel, B.-C.
Polynomial root finding.
IEEE Signal Processing Letters, **1**, 10 (Oct. 1994), 141–143.

[51] Sitton, G. A., Burrus, C. S., Fox, J. W., and Treitel, S.
Factoring very-high-degree polynomials.
IEEE Signal Processing Magazine, **20**, 6 (Nov. 2003), 27–42.

[52] Strobach, P.
The recursive companion matrix root tracker.
IEEE Transactions on Signal Processing, **45**, 8 (Aug. 1997), 1931–1942.

[53] Franklin, G. F., Powell, J. D., and Workman, M.
Digital Control of Dynamic Systems (3rd ed.). Boston: Addison-Wesley Longman, 1998.

[54] Stoica, P., and Nehorai, A.
Performance study of conditional and unconditional direction-of-arrival estimation.

IEEE Transactions on Acoustics, Speech, and Signal Processing, **38**, 10 (Oct. 1990), 1783–1795.

[55] Janssen, P. H. M., and Stoica, P.
On the expectation of the product of four matrix-valued Gaussian random variables.
IEEE Transactions on Automatic Control, **33**, 9 (Sep. 1988), 867–870.

[56] Gao, F., and Gershman, A. B.
A generalized ESPRIT approach to direction-of-arrival estimation.
IEEE Signal Processing Letters, **12**, 3 (Mar. 2005), 254–257.

[57] Sidiropoulos, N. D., Bro, R., and Giannakis, G. B.
Parallel factor analysis in sensor array processing.
IEEE Transactions on Signal Processing, **48**, 8 (Aug. 2000), 2377–2388.

Guangmin Wang (S'11) received the B.E. degree in information and communication engineering from Xi'an Jiaotong University, Xi'an, China, in 2008.

He is currently working toward the Ph.D. degree with the Department of Control Science and Engineering, Xi'an Jiaotong University, Xi'an, China. His current research interests include array and statistical signal processing.

Jingmin Xin (S'92—M'96—SM'06) received the B.E. degree in information and control engineering from Xi'an Jiaotong University, Xi'an, China, in 1988 and the M.S. and Ph.D. degrees in electrical engineering from Keio University, Yokohama, Japan, in 1993 and 1996, respectively.

From 1988 to 1990, he was with the Tenth Institute of Ministry of Posts and Telecommunications (MPT) of China, Xi'an. He was with the Communications Research Laboratory, MPT of Japan, as an Invited Research Fellow of the Telecommunications Advancement Organization of Japan (TAO) from 1996 to 1997 and as a Postdoctoral Fellow of the Japan Science and Technology Corporation (JST) from 1997 to 1999. He was also a Guest (Senior) Researcher with YRP Mobile Telecommunications Key Technology Research Laboratories Company, Limited, Yokosuka, Japan, from 1999 to 2001. From 2002 to 2007, he was with Fujitsu Laboratories Limited, Yokosuka, Japan. Since 2007, he has been a Professor at Xi'an Jiaotong University. His research interests are in the areas of adaptive filtering, statistical and array signal processing, system identification, and pattern recognition.

Jiasong Wang graduated from the astronomy department, Nanjing University, China in 1990, and received the M.S. degree in satellite orbit dynamics from Nanjing University in 1996 and the Ph.D. degree in civil engineering and geosciences from Newcastle University, UK, in 2004.

He joined Xi'an Satellite Control Center in 1990, and is currently a research fellow and vice director of the State Key Laboratory of Astronautic Dynamics in China. His research concentrates on satellite orbit determination, precise satellite navigation, space geodesy, and geophysical inferences from satellite orbit perturbations.

Dr. Wang has been a member of the orbit expert panel for Chinese manned spaceflight engineering since 2007 and a member of the expert group for the Chinese high resolution Earth observation project since 2011.

Nanning Zheng (SM'93—F'06) graduated from the Department of Electrical Engineering, Xi'an Jiaotong University, Xi'an, China, in 1975, and received the M.S. degree in information and control engineering from Xi'an Jiaotong University in 1981 and the Ph.D. degree in electrical engineering from Keio University, Yokohama, Japan, in 1985.

He jointed Xi'an Jiaotong University in 1975, and he is currently a Professor and the Director of the Institute of Artificial Intelligence and Robotics, Xi'an Jiaotong University. His research interests include computer vision, pattern recognition and image processing, and hardware implementation of intelligent systems.

Dr. Zheng became a member of the Chinese Academy of Engineering in 1999, and he is the Chinese Representative on the Governing Board of the International Association for Pattern Recognition. He also serves as the President of the Chinese Association of Automation.

Akira Sano (M'89) received the B.E., M.S., and Ph.D. degrees in mathematical engineering and information physics from the University of Tokyo, Japan, in 1966, 1968, and 1971, respectively.

In 1971, he joined the Department of Electrical Engineering, Keio University, Yokohama, Japan, where he was a Professor with the Department of System Design Engineering until 2009, and he is currently Professor Emeritus of Keio University. He is a member of the Science Council of Japan since 2005. He was a Visiting Research Fellow at the University of Salford, Salford, UK, from 1977 to 1978. His current research interests are in adaptive modeling and design theory in control, signal processing and communication, and applications to control of sounds and vibrations, mechanical systems, and mobile communication systems.

Dr. Sano is a coauthor of the textbook *State Variable Methods in Automatic Control* (Wiley, 1988). He received the Kelvin Premium from the Institute of Electrical Engineering in 1986. He is a Fellow of the Society of Instrument and Control Engineers and is a Member of the Institute of Electrical Engineering of Japan and the Institute of Electronics, Information and Communications Engineers of Japan. He was General Co-chair of the 1999 IEEE Conference of Control Applications and an IPC Chair of the 2004 IFAC Workshop on Adaptation and Learning in Control and Signal Processing. He served as Chair of IFAC Technical Committee on Modeling and Control of Environmental Systems from 1996 to 2001. He has also been Vice Chair of IFAC Technical Committee on Adaptive Control and Learning since 1999 and has been Chair of IFAC Technical Committee on Adaptive and Learning Systems since 2002. He was also on the Editorial Board of *Signal Processing*.